Scale effect of cavity expansion in soil with application to plant root growth

A thesis for the doctor degree submitted to

University of Natural Resources and Life Sciences, Vienna

submitted by

Samira Ladjal, Mag.

under the supervision of

Prof. Dr.-Ing. Wei Wu

Institute of Geotechnical Engineering

Department of Structural Engineering and Natural Hazards

A la mémoire de mon père

Acknowledgments

First of all I would like to express my gratitude and appreciation to my supervisor, Prof. Wei Wu for his valuable suggestions, helpful guidance, encouragement and for giving me the opportunity to work within such an interesting research field.

Furthermore, I would like to thank my committee members for they have been kind enough to be a part of this work.

I also gratefully acknowledge the financial support of this study provided by the Austrian Oriental Society. Many thanks go in particular to Dr. Theresia Laubichler for the kindness, friendship and support.

Many thanks also to all the colleagues and friends at our institute. My special thanks go to Dr. Markus Rauchecker for providing me the laboratory facilities. I would also like to thank Dr. Gerhard Sinn, from the laboratory of physics and materials science for helping me to use of Zwick/Roell testing machine.

Finally, I owe much to my family. Their encouragement is not only important but also indispensable to my study and life.

Abstract

A procedure for analyzing the expansion of spherical cavities in cohesive-frictional and in cohesionless materials is described. The aim is to provide a theoretical framework based on a constitutive law with high-order strain gradient, which takes the microstructure of soil into consideration. It is demonstrated that the penetration pressure required to expend a cavity in soil depends on the ratio between the cavity size and the mean grain diameter of the soil particles. The need for these high-order formulations originates from the inability of the classical plasticity framework to account for the underlying microstructure and to explain the observed size effects. According to the classical theory of cavity expansion, the expansion pressure remains independent of the cavity size since the governing equations is written in a dimensionless form, predicting for all the geometrically similar cavities the same limit pressure. To validate the theory, laboratory experiments with 2, 5 and 10 mm penetrometer diameters are performed on loose and dense sand. Comparison between experimental results and calculations yields a good agreement for the penetration cone resistance with coefficients of determination of 0.97 and 0.85 for loose and dense sand respectively .

The above theoretical models have some interesting implications for the growth of root in soil with high impedance. The seminal roots of most plants thicken when growing into soil with higher mechanical impedance. This study provides a further explanation to root thickening, an increase in root diameter may give rise to reduced

penetration pressure. This implies that enhanced penetration can be obtained by root thickening even when the turgor pressure remains unchanged.

Zusammenfassung

Ein neues Verfahren zur Untersuchung der Aufweitung sphärischer Hohlräume in Materialien mit und ohne Kohsion wird beschrieben. Das Ziel ist die Erstellung eines theoretischen Rahmenkonzepts, basierend auf einem Stoffgesetz mit Verformungsgradienten höherer Ordnung, welches die Mikrostruktur des Bodens berücksichtigt. Wir zeigen, dass der notwendige Eindringungsdruck eines Penetrometers um einen Hohlraum im Boden zu erweitern vom Verhältnis zwischen Hohlraumgröße und dem mittleren Korndurchmesser abhängig ist. Die Notwendigkeit für die Formulierung höherer Ordnung resultiert aus der Tatsache, dass die klassische Plastizitätstheorie keine charakteristische Länge besitzt. Die klassische Theorie ist nicht in der Lage, die zugrunde liegende Mikrostruktur zu berücksichtigen sowie beobachtete Größeneffekte zu erklären. Nach der klassischen Theorie bleibt der Grenzdruck bei der Hohlraumaufweitung unabhängig von der Hohlraumgröße, da die zugrunde liegenden Gleichungen dimensionslos formuliert sind, und dementsprechend für alle geometrisch gleichen Hohlräumen den gleichen Grenzdruck liefert. Zur Validierung der neuen Theorie wurden Laborversuche mit 2, 5 und 10 mm Penetrometer Durchmesser in lockerem und dichtem Sand durchgeführt. Der Vergleich zwischen Experimenten und Berechnungen zeigt gute Übereinstimmung des Penetrationsgrenzdrucks mit Korrelationskoeffizienten von 0.98 und 0.85 für den lockeren bzw. dichten Sand.

Das beschriebene theoretische Model hat interessante Folgerung für Wurzelwachstum in Böden mit hohem Widerstand. Es ist bekannt, dass sich Seminalwurzeln

der meisten Pflanzen in Böden mit hohem mechanischen Widerstand verdichten. Unsere Untersuchung bietet eine interessante Erklärung für die Wurzelverdickung. Eine Erhöhung des Wurzeldurchmessers reduziert den Eindringungsdruck. Dies bedeutet, dass die Wurzelverdickung ein verbessertes Eindringen ermöglichen kann, sogar bei gleichbleibendem Turgordruck.

List of Figures

List of Tables

Contents

Chapter 1

Introduction

The growth of plants depends on the capability of their roots to penetrate through soil to acquire water and nutrient. Growing roots are often subjected to various unfavorable conditions with the mechanical impedance of soil being the major factor limiting root growth. The soil mechanical impedance is usually described in terms of soil strength, which is defined as the amount of force required to move or rearrange soil particles. In addition to being dependent on textural and mineralogical properties, soil strength is also strongly dependent on soil moisture content, increasing rapidly with decreasing soil water content. The most common way to assess soil strength is to use a soil penetrometer, which characterizes the force needed to drive a cone of specific size into the soil. Most of the experimental work on the axial forces developed by roots has been closely associated with penetrometer testing (e.g. Barley, Farrell and Greacen, 1965; Cockroft, Barley and Greacen, 1969; Whiteley and Dexter 1981; Bengough and Mullins, 1990a; Bengough, Mullins and Wilson, 1997). Measurements on soil with penetrometer suggest that root elongation rate is not so affected by impedance until the penetrometer resistance reaches about 0.3 MPa (Taylor and Burnett, 1963). By direct measurement of both penetrometer resistance and root growth, Stolzy and Barley (1968) found that the axial pressure exerted by

two pea roots was only 80% of that exceeted by a probe of 1 mm diameter. Bengough and Mullins (1991) found that the soil resistance to the 1 mm diameter probe was between about 4.5 and 7.5 times greater than the measured penetration resistance to maize roots. This difference between root and probe resistance may be due to a combination of the root-soil friction being smaller than the soil-metal friction, but also to the faster rate of penetration of the penetrometer probe (some 65-120 times faster) (Iijima et al., 2003).

In order to penetrate through soil, roots have to displace soil particles. Theoretically, a growing root exerts radial and axial pressures onto soil (Misra, Dexter and Alston, 1986a). Consequently, the soil should be denser around and in front of the growing root than in far field (Dexter, 1987). X-ray photography used to illustrate the increase in soil density near the root-soil interface shows that the deformation around the holes made by roots and fine penetrometers is almost cylindrical, with a small spherical component in the front of the tip (Greacen, Farrell and Forrest, 1967; Greacen and Sands, 1980).

Root penetration was studied as cavity expansion by Farrell and Greacen (1966). They assume that the pressure on the base of a probe is equal to the pressure required to form a spherical cavity in the soil. This pressure was explained in terms of shear strength, cohesion, friction and critical state compressibility of the soil. A similar analysis was carried out by Misra, Dexter and Alston, (1986b, 1986c) based on the theory of cavity expansion by Vesic (1972). The soil surrounding the root was modeled by an elastic, perfectly plastic material.

In soil science, penetration tests are used to characterize the compaction of agriculture soils. The penetrometers have typically a diameter between 10 cm and 20 cm, which are much larger than the usual root diameter of agriculture plants (between 0.2 mm and 2 mm). Theoretical work on the deformation of soil by penetrometer

probes assumed that the soil strength was unchanged in the proximity of the root tip (Farrell and Greacen, 1966). However, some laboratory tests with small penetrometers show clear dependence of the penetration pressure on the penetrometer diameter (Whiteley and Dexter, 1981, Figure 1.1a). A similar effect was showed by Bolton et al. (1999) (Figure 1.1b). The tests by Bolton and his co-workers were carried out in a geotechnical centrifuge at an acceleration of 70g. The soil used by Whiteley and Dexter is a silty soil with a mean grain diameter of about 0.1 mm. The specimen was prepared by remolding the soil at the water content close to its plastic limit of about 17.3%. The soil used by Bolton and his co-workers is clean sand with a mean grain diameter of about 0.9 mm. The penetration resistance in Figure 1.1a is obtained by normalizing the penetration force with the cross-section area of the penetrometers. The normalized resistance in Figure 1.1b is defined by ratio between the penetration pressure and the overburden stress. In both tests the penetration resistance decreases with increasing penetrometer diameter. For large diameter the penetration resistance is expected to approach a limit value, which can be obtained from the classical theory of cavity expansion. Obviously this scale dependence cannot be predicted by the classical theory, since the constitutive equation does not contain any term with length scale.

In order to account for the scale effect, it is therefore essential to enrich the classical description of the environment through additional terms that reflect the phenomena occurring at the scale of the microstructure. Recently, material modeling including microstructure characteristics has been extensively discussed in literature. This models are traditionally divided into the *Cosserat* models, where rotational degrees of freedom are added to the conventional translational degrees of freedom (Mühlhaus and Vardoulakis, 1987); *integral-type* nonlocal models, which use spatial weighted averages (Bažant and Pijaudier-Cabot, 1987) and *gradient* models, which

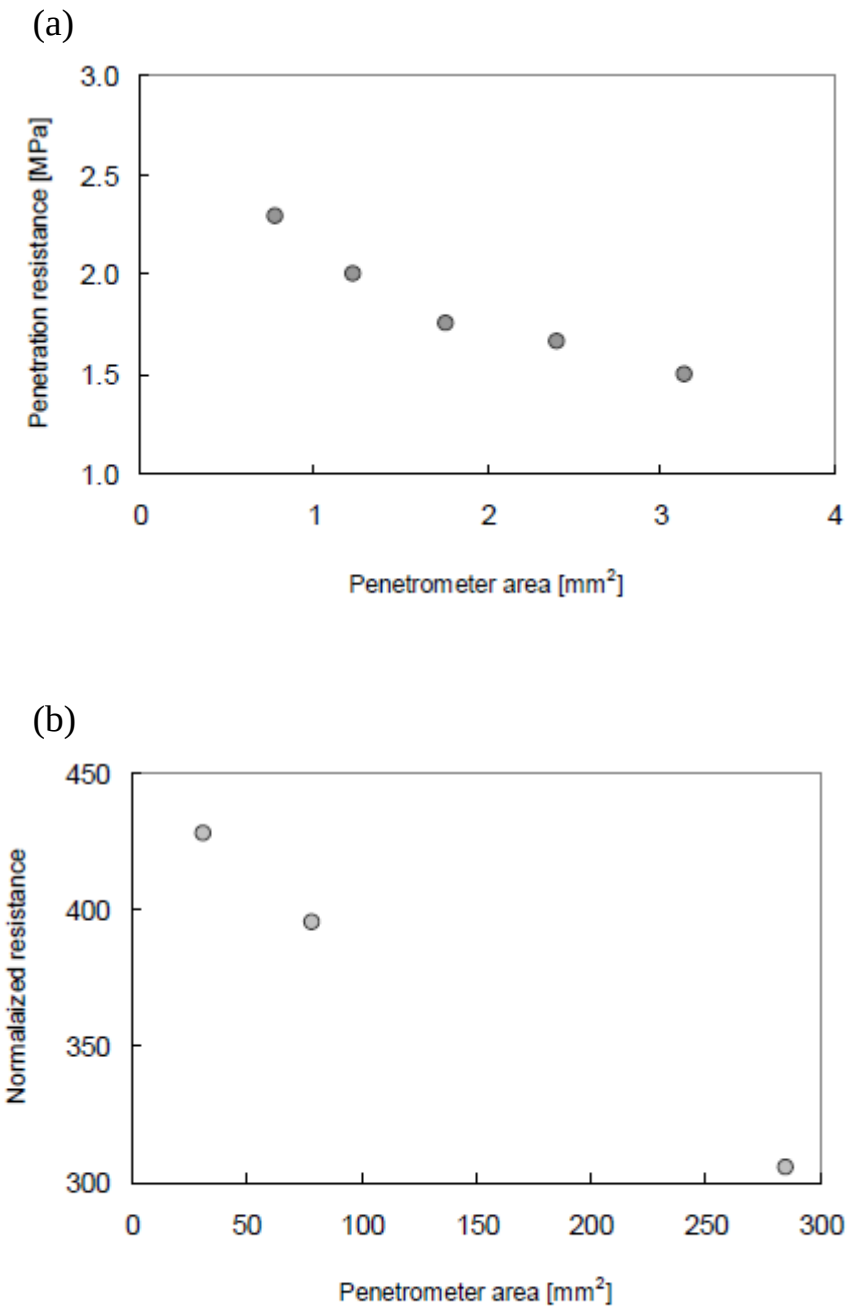

Figure 1.1: Penetration tests (a) by Whiteley and Dexter (1981) and (b) by Bolton et al. (1999)

work with differential operators (Vardoulakis and Aifantis, 1991). An interesting feature of the gradient plasticity models is that the presence of spatial gradients of the state variables necessitates additional boundary conditions for the relevant quantities on the boundary of the plastic zone (Mühlhaus and Aifantis, 1991).

In this study we use an enhanced constitutive equation with high-order strain gradient to simulate the penetration of plant roots into compacted soils. An internal length parameter is incorporated, which can be related to some material properties like the mean grain diameter of soil. A natural way to incorporate such a length scale into the constitutive law is to postulate that the yield strength depends upon both strain and strain gradient. Considering that root growth is analogous to the expansion of spherical cavity, this mechanical model can be used to explain some scale effect in the interaction between plant root and soil. The soil is modeled as an elastic-perfectly plastic material. Its response in the elastic region is assumed to obey the Hooke's law. Yielding is determined by the Drucker-Prager yield criterion. In order to test the model formulation, a comparison is made of penetrometer resistance measurements obtained from laboratory experiments, using probes of different sizes, with the theoretically predicted cavity expansion pressures, which are based on the gradient approach.

The thesis is organized as follows. Chapter two presents a review of the variation in the morphology and architecture of root systems and focuses on the responses of roots to increased mechanical impedance. Chapter three gives an overview of the necessary framework of the local plasticity theory which serves as the background for the development of the gradient plasticity theory and presents some example of the application of gradient plasticity in localization and size effects problems. Chapter four describes the application of a Drucker-Prager gradient plasticity model of the form used by Vardoulakis and Aifantis (1991) to cavity expansion problem.

Analytical models, for cohesive-frictional and for cohesionless soils, are developed and used to simulate the penetration of plant roots into the soil. Chapter five presents the results of laboratory experiments on penetrometer with diameter 2, 5 and 10 mm and discusses the comparison between these results and the theoretical predictions. Chapter 6 presents a summary of the research, and look into some possible research extensions.

Chapter 2

Soil compaction and root growth

2.1 Introduction

An important factor controlling the growth and yield of plants is the ability of the roots to penetrate through soil to acquire water and nutrients, which in turn has substantial influence on the development of shoots and yields. The penetration of a single root depends on the internal properties of the root as well as external environment conditions (Greacen and Oh, 1972). Where existing soil pores are smaller than the root diameter, roots are mechanically impeded. Consequently, the growth rate of the individual roots will be reduced, the diameter of roots increased and the pattern of branching altered (Bengough and Mullins, 1990b).

This chapter aims to describe the soil mechanical properties such as the compaction and soil strength, reviews the essential anatomical and morphological features of roots as a background to understand the diverse forms of root systems and, concentrates on some of the responses of roots and root systems to soil mechanical properties.

2.2 Soil compaction

Compaction is an increase in soil bulk density and reduction in pore space, associated usually with an increase in soil strength (Whalley, Dimitru and Dexter, 1995). These phenomena results from the rearrangement of soil particles under the weight of agricultural machinery and animals. Compaction changes the size and the shape of aggregates and clods, and therefore the total porosity, pore shape and pore size distribution, which restrict air and water movement into and through the soil. The degree of soil compaction that may be obtained is related to the soil structure, soil texture and to the moisture and organic matter content. For mixtures of fine sand and a silty clay soil, the maximum density for a range of prepared soils is shown in Table 2.1 (Bodman and Constantin, 1965. Cited by Greacen and Sands, 1980). The data show the dependence of the bulk density on the soil texture. The bulk density tends to be lower in soils with higher contents of clay. Soil compaction can affect

Table 2.1: Data for fine sand/silty clay mixtures

Texture:	Silty clay	Clay loam	Sandy clay loam	Sandy loam	Loamy sand
Sand/silty clay	0/100	20/80	40/60	60/40	80/20
ρ (g/cm^3)	1.42	1.53	1.69	1.77	1.85
Clay (%)	50	40	30	20	10
Liquid limit (%)	57	50	43	37	30
Plastic limit (%)	27	26	25	24	23

plant growth by impacting soil physical, chemical and biological properties. This properties moderate the growth rate of the root axes, which may be accompanied by morphological and physiological changes to the root system (Clark, Whalley and

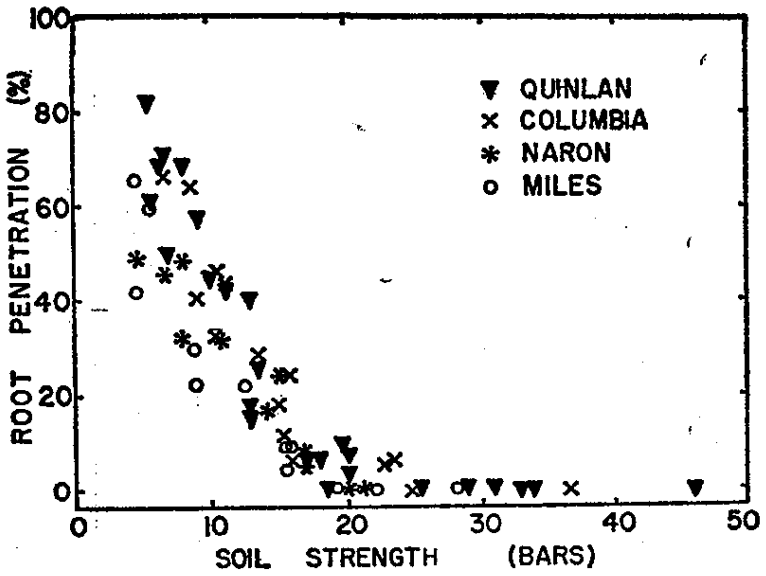

Figure 2.1: Relation between the soil strength and percentage of cotton taproots penetrating through cores of four soils. (From Taylor, Roberson and Parker (1966)).

Barraclough, 2003). To assess the effects of soil compaction on the root growth, some measurements of soil strength and bulk density can be useful. For example, Taylor, Roberson and Parker (1966) reviewed study describing rooting patterns of cotton seedling taproots in four different soil that ranged in texture from loam to loamy sand. They found that high bulk densities, which are varied with soil texture, greatly reduce the rooting of cotton seedling taproots (Figure 2.1). They found also that for Columbia loam compacted to bulk density of about 1.3 g/cm^3 and at 2/3 bars soil suction, the soil strength, which was about 10 bars, was sufficient to reduce by more than a half the number of roots penetrating the soil.

2.3 Soil strength

As a result of excessive external stresses, soil undergo irreversible deformation manifested by the sliding of grain over each other. At failure, the shear stress of the soil

(in fact the skeleton) is called the ultimate strength or shear failure.

Coulomb (1776) was the first to define an expression for the shear strength of granular materials, according to the connections that exist between the grains forming the skeleton (connections due to the capillary pressures caused by the interstitial water content and adsorbed) and skeletal structure (shape and arrangement of the grains). This expression is given by the following equation

$$\tau = c + \sigma \tan \varphi \tag{2.1}$$

where τ is the shear stress needed to cause failure, c and φ denote the cohesion and angle of internal friction of the soil (shear parameters) and σ is the normal stress acting on the failure plane.

Cohesion and internal friction angle are intrinsic properties of the material that depend on the mineralogy, particle size distribution and geological history. These two parameters take specific values when the material is purely frictional ($c = 0$) or purely cohesive ($\varphi = 0$). Between these two extreme values, several materials are found that have properties intermediate as is the case for most natural soils.

2.4 Measuring soil strength

Experimental studies (laboratory and in situ) on the behavior of soils are primarily intended to provide data on strength and deformability of soils. Various devices can be used to measure the soil strength. They include the triaxial cell, the direct shear box, the unconfined compression machine, shear vane and penetrometer.

Traixial load cells are devises, in which a hydrostatic pressure is radially applied and an additional axial force can be applied to a soil sample. In the direct shear test, the soil sample is placed into a shear box. Whilst a normal force is applied, the bottom box is moved sideways. Unlike the triaxial test in which various stress

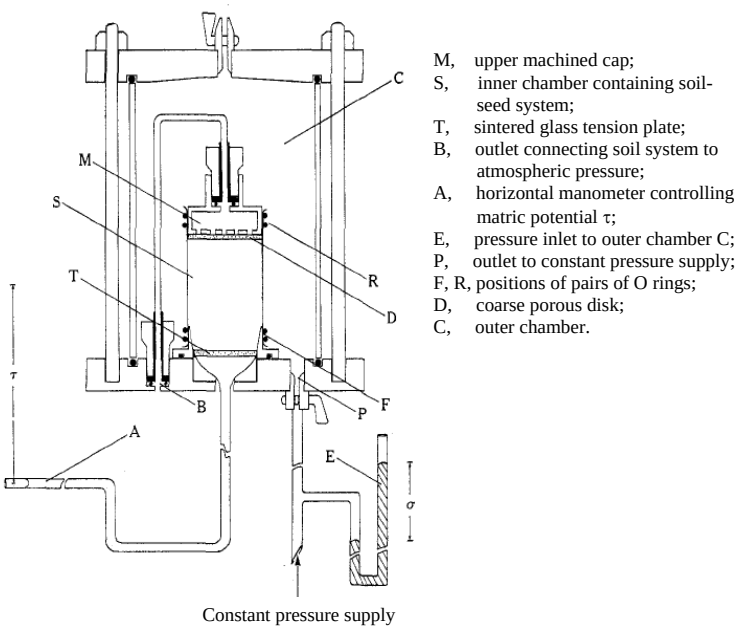

Figure 2.2: Schematic diagram of modified triaxial cell used by Collis-George and Williams (1968)

paths (or strain) can be followed, the direct shear test is carried out with a failure plane imposed in horizontal direction.

The triaxial cells were modified by many researchers to study the growth of roots under various stress conditions (e.g. Collis-George and Williams, 1968; Abdalla, Hettiaratchi and Reece, 1969). The triaxial apparatus used by Collis-George and Williams (1968) was designed to study the germination of Lactuca sativa by varying independently the matric potential and the effective isotropic stress Figure 2.2). Abdalla, Hettiaratchi and Reece (1969) have modified the triaxial cell that no provision is made for the deviator stress. The top cap was modified to allow the shoot to grow out of the rooting medium. The lower end of the cylinder is closed and has tappings for aeration of the sample and the supply of a nutrient solution. Later, Richards and Greacen (1986) used a modified cell with a small expanding latex tube, which simulates the growing root.

In the unconfined compression test, a soil specimen is placed between two platens,

one of which is fixed and the other movable. A vertical force is then applied. The force at failure is divided by the cross-sectional area to give the unconfined compressive strength. Compared with the triaxial test, it is not possible to explore the behavior under three dimensional stress condition.

Vane shear test gives the shearing resistance of cohesive soils. The vane is pushed vertically into the ground and then rotated. The maximum torque (force times lever arm) required to rotate the vane is divided by the surface area of the sheared cylinder. Vane test results can be severely affected by macro-fabric and the undrained conditions assumed may not valid if the soil contains permeable layers.

The penetrometer, in both versions with and without measurement of pore watter pressure, is the most commonly used device for measuring the strength characteristics of soils. The penetrometer consists typically of a cylindrical rod with a conical tip at one end, and a device for measuring the force at the other (Figure 2.3). The penetration resistance is the force required to push the cone into the soil divided by the cross sectional area of its base. Most studies on the effects of compaction on root growth are based on penetration tests. Root growth rate decreases with increasing soil resistance to penetration. The growth rate is often found to approach minimum values when the soil resistance, as measured with a penetrometer, reaches about 2 MPa (Taylor, Roberson and Parker, 1966).

As the probe penetrates the soil, it deforms the soil creating a cavity. The shape of this cavity is intermediate between a sphere and a cylinder depending on the shape of the cone (Greacen and Sands, 1980). Farrell and Greacen (1966) reviewed the mechanics of soil failure associated with the penetration. They pointed out that the expansion of the cavity took place through compression of the soil around the penetrometer. In the plastic zone sorrounding the penetrometer, there are three distinct subzones. In zone I, the soil is compressed to its optimum density (minimum

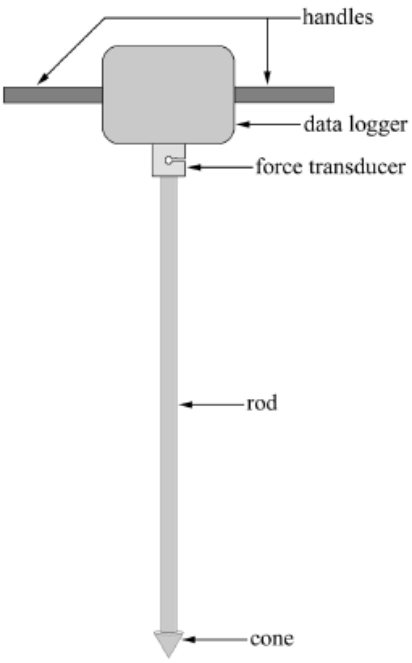

Figure 2.3: Schematic diagram of a penetrometer

void ratio), while in zone II, the soil undergoes failure and zone III is a rebound zone, where the soil behaves as an overconsolidated material. Outside this, is a zone of elastic compression. As such, the penetration resistance consist of two components: the pressure required to expand the cavity in the soil, and a frictional resistance to the probe, so that

$$q_c = \sigma(1 + \tan\phi \cot\alpha) \tag{2.2}$$

where σ is the normal stress acting on the cone surface, calculated from the cavity expansion models in soil, ϕ is the soil-metal friction angle and α is the semi-angle of the cone probe. Blunt penetrometer (probe with large cone angles) is related to spherical cavity expansion, whereas cylindrical cavity is related to finely tapered probes (probe with narrower cone angles) (Greacen and Sands, 1980). An additional correction for Equation 2.2 was proposed to take the effect of soil-metal adhesion on

the cone surface, noted c_a into account (Bengough, Campbell and O'Sullivan, 2001):

$$q_c = \sigma(1 + \tan\phi \cot\alpha) + c_a \cot\alpha \tag{2.3}$$

This equation assumes that the soil is homogeneous and isotropic, that the soil-shaft frictional resistance is negligible, that no soil-body accumulates in front of the cone and that the stress is distributed uniformly on the cone surface.

Correlations between roots and penetrometers show that the resistance experienced by penetrometers is much larger than that experienced by roots. This may be due to the different tip geometries of penetrometers and roots but also to the low root-soil friction (Bengough, Mullins and Wilson, 1997). Moreover, roots are flexible organs, which tend to change their morphology in response to increasing soil strength (Whalley, Dumitru and Dexter, 1995).

2.5 Root systems

Angiosperms, or flowering plants, are the plant group of major importance for agricultural use. The angiosperms contains two main classes: monocotyledons and dicotyledons. Anatomical and physiological differences between these groups are found in most plant organs, in the shoot as well as the root system.

The primary functions of the roots are anchorage of the plant in the soil and acquisition of water and nutrients (Fitter, 1996). which in turn has substantial influence on the development of shoots and on crop yield. People are less familiar with roots than the more visible flowers, stems, and leaves, but roots are no less important to the plant.

Different plant species show different root structures (Figure 2.4). Most monocotyledonous plants, such as grasses, have fibrous root systems. This is usually formed by thin, moderately branching roots growing from the stem. In many di-

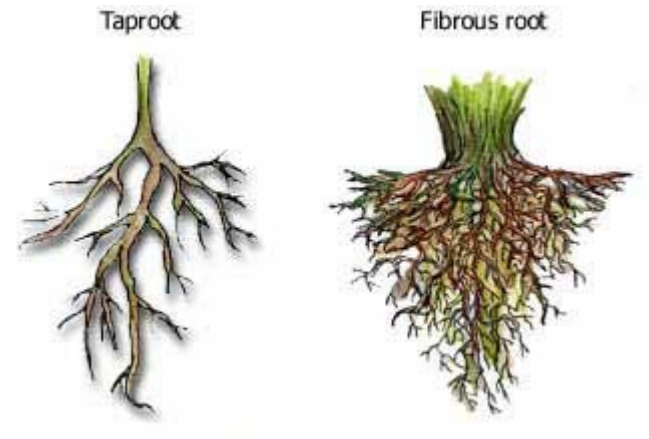

Figure 2.4: Plant root systems: the taproot system and the fibrous root system.

cotyledonous plants, the root enlarges greatly to become the most prominent root of the plant and is known as a taproot. The taproot develops directly from the radicle and produces branch called lateral roots (Nabors, 2004).

Materechera, Dexter and Alston (1991) showed that the dicot roots, which have the largest diameter, are better at penetrating compacted soil layers than monocots. This could be related to the effects which root diameter may have on root growth pressure and on the mode of soil deformation during penetration (Materechera et al., 1992). These results are consistent with those of Mitchell, Ellsworth and Meek (1995), who also showed that the size of the taproot is more important for the creation of large continuous biopores, which are effective in water transport and soil aeration.

Internally, the roots of all cultivated plants are built on the same general plan and differ from one another only in detail (Figure 2.5). The principal features which distinguish dicot from monocot roots include the vascular arrangement with its star-shaped xylem in the stele and the occurrence of significant secondary growth (Klepper, 1992). In dicotyledonous plant roots, between the xylem and phloem, is

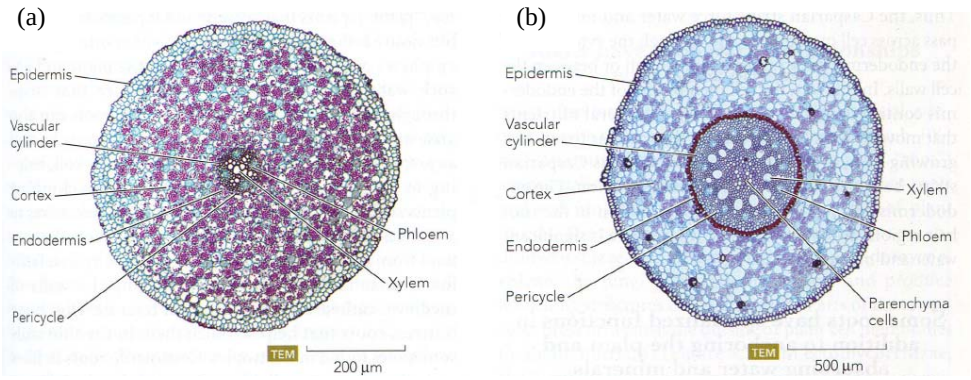

Figure 2.5: Cells of a: (a) dicot and (b) monocot roots cut in transverse section (Nabors, 2004).

a layer of very small meristematic cells called the vascular cambium. These cells can divide to produce new xylem and phloem. In this way, the vascular cambium is responsible for the increase in root diameter. Dicotyledons also form another zone of meristematic cells in the pericycle, the cork cambium, at about the same time. The increase in diameter of most monocotyledons roots results from elargement of cells produced in the apical meristem because a vascular cambium is absent in the majority of those plants (Dickison, 2000).

The root grows mainly from its tip. As cells are added to the tip by repeated cell divisions, a young root elongates and leaves behind cells that differentiate and become the primary roots of the plant. Four areas of the young root are traditionally recognized. These regions, starting at the tip and moving upwards towards the stem, are the root cap, zone of active cell division, zone of cell elongation, and zone of differentiation (Figure 2.6). The exact positions of the last three zones can vary between species, growth conditions and tissue layers (Leyser and Day, 2003).

The root cap is thought to be a source of lubrication to the growing root apex, and a means of causing adherence of mature roots to soil particles via the production of

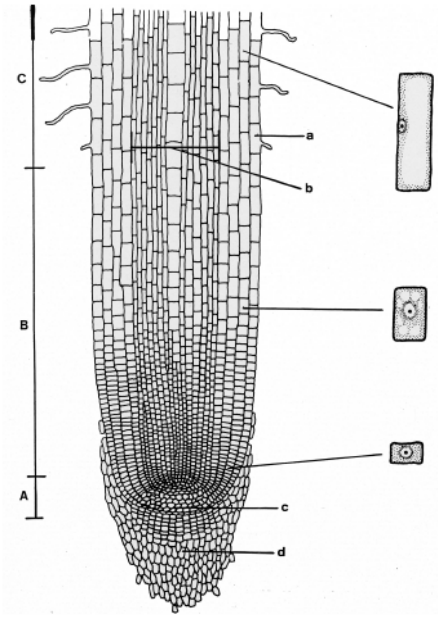

Figure 2.6: The zones of (A) root cap , (B) cell division (C) cell elongation and (D) cell differentiation in a longitudinal cut of a maize root. (a) epidermal cell with a root hair, (b) stele, (c) apical meristem and (d) root cap.

mucilage (Raven and Edwards, 2001). The root cap initially defines the rhizosphere by its direction of growth, which in turn occurs in response to gradients in soil conditions and gravity (Hawes et al., 2003). Furthermore, it plays also an important role in the regulation of root growth rate as affected by mechanical impedance (Bengough and Mullins, 1990b).

Just behind the root cap, there is a meristematic zone in which the cells are in a state of active division. Above that is the zone of elongation. The cells located in this region undergo elongation and enlargement and are responsible for growth of root. After elongation, the cells differentiate into the typical cell type associated with the specific location (Forbes and Watson, 1992).

2.6 Root responses to mechanical impedance

The response of roots to mechanical impedance has been addressed largely in the literature (e.g. Barley, 1963; Barley and Greacen, 1967; Atwell, 1988). Generally, mechanically impeded roots are shorter, thicker than roots grown in loose soil (Bengough, 2003). Studies such as that of Veen (1982) indicate that exposing maize roots to 40 kPa of pressure resulted in a 75% reduction in root length and a 50% increase in root diameter. These changes in morphology of impeded roots have been attributed to both an increase in diameter and the reduction in length of the cortex cells (Atwell, 1988; Pritchard, 1994). Generally, roots of different species may vary in their ability to penetrate through compacted soil (Materechera, Dexter and Alston, 1991). This is largely relevant to the thickness of the roots and their tendency to swell in response to mechanical impedance (Atwell, 1988; Materechera, Dexter and Alston, 1991; Materechera et al., 1992)

2.6.1 Growth pressure

Roots grow by a process of cell division in the apical meristem just behind the tip, and cell expansion in a zone just behind the apex (Clark, Whalley and Barraclough, 2003). The rate of this expansion r is often analyzed in terms of the Lockhart equation as

$$r = m(P - Y) \tag{2.4}$$

where m is the extensibility of the cell wall, P is the turgor pressure, and Y is a minimum value of P below which the cell will not grow. Assuming that the permeability of the cells to water is not limiting cell expansion, Greacen and Oh (1972) modified the equation of Lockhart to include the root penetration resistance

of the soil σ, such that

$$r = m(P - Y - \sigma) \tag{2.5}$$

If the root is completely impeded, so that the elongation rate is zero, σ reaches a maximum. The maximum growth pressure that a root can exert is given by setting $r = 0$ in equation (2.2).

The first measurements of the growth pressure were reported by Pfeffer (1893). Since then, many authors have addressed this problem (e.g. Greacen and Oh, 1972; Aggarwal and Prihar, 1975; Misra, Dexter and Alston, 1986a; Souty, 1987; Clark et al., 1999). The maximal pressure that can be exerted by roots is ultimately limited by the turgor pressure in the expanding cells of the root elongation zone (Clark et al., 1999) which is determined by the osmotic potential in the cell vacuole (Bengough, Croser and Pritchard, 1997). Greacen and Oh (1972) suggested that root cells may change their osmotic potential to exert more pressure on the surrounding soil. Atwell (1988) found an increase of about 27% in the osmotic pressure of lupin roots growing in compacted sandy clay loam. However, Bengough, Croser and Pritchard (1997) suggested, from measurements of the cell osmotic potential of mechanically impeded roots, that the cell wall properties were more important than turgor in regulating the elongation rate of roots. They emphasized that P, m and Y in (2.4) are not constants, but are physiological properties that depend on the root environment. Moreover, several researchers (e.g. Goss and Russell, 1980; Veen, 1982) suggested that the response of root growth in compacted conditions is hormone mediated and indicated that ethylene may play a role.

Based on measurement in pea, cotton and sunflower, Misra, Dexter and Alston (1986a) reported that the maximal root growth pressure σ_{max} was found to increase with increasing root diameter. Materechera et al. (1992) suggested also that thicker roots exert higher axial pressure. But, Clark and Barraclough (1999) found no

significant difference in σ_{max} between dicots (with thicker roots) and monocots. In general, roots with larger diameter have better ability to penetrate compact soil (Materechera et al., 1993).

2.6.2 The rate of elongation of roots

Higher soil strength decreases the elongation rate of roots (Figure 2.7). Barley (1963) simulated high soil strength by applying radial pressure to roots growing in fine-grained cohesionless material; the elongation rate fell sharply when the mechanical impedance was increased. Correlations between root elongation rate and root penetration resistance showed that soil with resistance of about 0.46 MPa can reduce the root elongation rate of pea root by 56% (Stolzy and Barley, 1968). Bengough, Mackenzie and Elangwe (1994) showed that when a compressive force is applied to seedling pea root, root elongation rate decreased by more than 50% within 30 min of increasing the applied force by 100 mN. A smaller increase in growth rate was observed when the force was removed. Based on measurement in mechanically impeded pea roots, Croser, Bengough and Pritchard (1999) found a decrease of the rate at which new cells are added onto a file (i.e. cell flux) and of the final cell length, which contributed to a slower elongation rate and a shorter zone of elongation.

The response of the root to mechanical impedance and the importance of the root tip in mediating the response were demonstrated by Goss and Russell (1980) by observing the response of the seminal axis of maize to small glass ballotini. They found that the elongation rate of intact maize roots was rapidly reduced by more than 70% for a period of 10 mminutes after contact with the glass bead, after which it gradually increased to the initial rate of elongation after 15 minutes. No change in the rate of elongation was observed in roots which had been decapped.

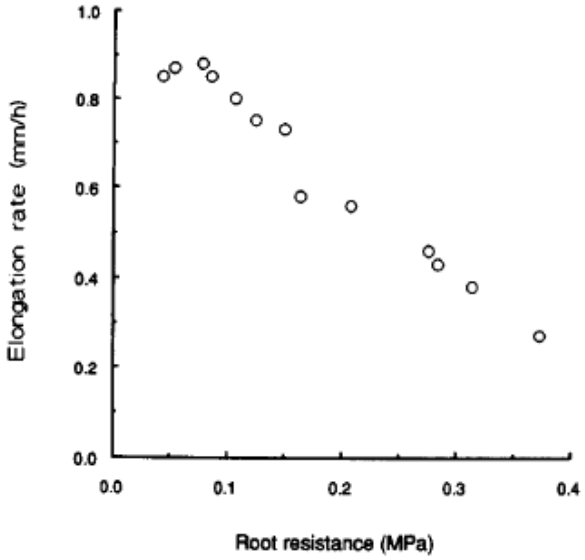

Figure 2.7: Root resistance versus elongation rate of pea seedling roots in remoulded cores of sandy loam soil calculated from Eavis (1967) by Bengough and Mullins (1991)

2.6.3 The swelling behavior of roots

The growth in compacted soils usually causes morphological changes of roots, such as larger diameter of roots due to a great enlargement in the cortex in which cells became shorter in longitudinal direction and wider across, while the stele remains constant in diameter (Iijima and Kato, 2007, Figure 2.8). In impeded pea roots, the number of cortical cell layers is increased from 7 to 10 (Croser, Bengough and Pitchard, 1999), while in lupin roots, the number of cortical cell layers remains unchanged (Atwell, 1988). Atwell (1988) showed that the radial swelling is primarily achieved by the yielding of tangential and radial cell walls of the outer cortex. A similar analysis was carried out by Croser, Bengough and Pritchard (2000), who found that the changes in cell morphology, which is not associated with a decrease in cell turgor, appears to be a loosening of cell walls in the radial direction and

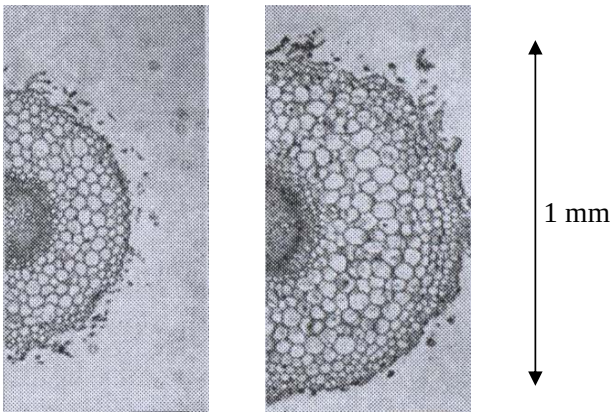

Figure 2.8: Cross section of cotton root under different soil densities: (a) 1.0 Mg/m^3, (b) 1,5 Mg/m^3. (From Iijima and Kato, 2007)

a stiffening of walls in the axial direction. In general, thicker roots have higher buckling resistance (Whiteley and Dexter, 1983b). Moreover, thicker roots may reduce the axial stress in front of the root tip (Abdalla, Hettiaratchi and Reece, 1969; Richards and Greacen, 1986).

2.6.4 The shrinking behavior of roots

In order to penetrate soil, which contains smaller pores than the tip of growing root, the root tip region must exert sufficient force to deform the soil. There is not much information about the minimum size of pore into which a root can grow without having to enlarge it (Gregory, 2006), but Wiersum (1957) suggested that the root penetration in such soil is possible only if the pore size exceed the root size. However, Scholefield and Hall (1985) showed that roots of some grasses e.g. reygrass, were able to penetrate into rigid pores of a smaller diameter than that of the root. Under their experimental conditions, seminal axes that were $880\mu m$ in diameter could penetrate rigid pores $\geq 315\mu m$. They found that the thickness

of the cortical cells was decreased, while the stele remains unchanged. The results of more recent studies of the growth of maize roots through rigid walls showed in contrast a thinning of both the cortex and stele (Bengough, Croser and Pritchard, 1997). Bengough and his co-workers suggested that this radial compression may affect the hydraulic conductivity of roots since the conducting area of xylem vessels is also decreased.

2.6.5 The branching of roots

Morphological changes in the root system may occur as a results of changes in soil compaction. Root systems growing in hard soil look very stunted compared with those grown in loose soil (Bengough, 2003). This may be due to the compression of soils around expanding roots, which lie within certain distances of root axes (Dexter, 1987). The effect of mechanical impedance on pea and seedling roots grown in compacted sandy loam (Barley, Farrell and Greacen, 1965) and on lupin roots grown in compacted sandy clay loam (Atwell, 1988) was studied. Barley and his co-workers found a decrease in the production of laterals. Atwell (1988) found little or no proliferation of laterals due to compaction and the zone of lateral root growth is sometimes advanced nearer to the apex of the main axis. Goodman and Ennos (1999) found also no significant difference in the number and weight of first-order laterals of sunflower and maize due to soil compaction. However, tests with artificial soil conditions suggest an increase in the number of lateral roots (Goss and Russell, 1980; Veen, 1982). This may be the result of larger pores being present in artificial conditions, which is not the case in compacted field conditions.

2.7 Soil heterogeneity and root growth

Much of the research on the effect of mechanical impedance on root growth has been concerned with the behavior of roots grown in artificial systems, such as glass, wax or sand compacted to a certain degree (Abdalla, Hettiaratchi and Reece, 1969; Goss and Russell, 1980; Bengough and Mullins, 1990b). Responses of roots to conditions in such laboratory environments may differ greatly from field, which include fine soil, clods, peds and biopores (i.e. root channels and earthworm tunnels). Such soil characteristics are not always favorable for root elongation because the mechanical impedance is not evenly distributed and its heterogeneity induces complex influence on root systems, plants, and on crop production. However, channels and cracks can allow the roots to overcome the areas of compacted soil, enabling access to a larger volume of soil with water and nutrients (Stirzaker, Passioura and Wilms, 1996). Moreover cracks narrower than the diameter of the root increase greatly the elongation of the root than in bulk soil, by reducing partially the mechanical impedance (Whiteley and Dexter, 1983a). Materechera et al. (1993) showed that the vertical biopores are important to the development of roots at depth.

However, excessively large pores and cracks in the soil, which have diameters many times that of the root, can also have a negative effect on root growth (Pierret, Moran and Pankhurst, 1999). This may be due to the poor soil-root contact, which decreases the ability of roots to extract water and nutrients, and perhaps even low level of growth inhibitors produced by root tip (Passioura, 2002). Furthermore the existence of continuous biopores gives rises to a clumped root distribution, due to the difficulties for laterals to penetrate the pore walls. Better plant growth was obtained when roots were grown in a network of narrow root channels made by lucerne and reyegrass (Stirzaker, Passioura and Wilms, 1996). Furthermore, lateral roots show better penetration of the biopore walls because of their orientation and

thickness (Whiteley and Dexter, 1983a).

2.8 Soil aggregate size and root growth

The ability of roots to penetrate soil depends mainly on the physical properties of soil, such as soil compaction (Atwell, 1990) and size and strength of soil aggregates (Misra, Alston and Dexter, 1988; Logsdon, Parker and Reneau, 1987). Donald, Kay and Miller (1987) sieved aggregates of different sizes (less than 1.6 mm, 1.6 to 3.2 mm, 3.2 to 6.4, 6.4 to 12.8 mm) from a loam to obtain different growing media. They found that maize plants growing in pots filled with the smallest of the aggregates grew substantially better than plants growing in the larger aggregates. Misra, Alston and Dexter (1988) reported also, for cotton and sunflower plants grown in pots containing aggregates of 6 different sizes (ranging from 1 to 19 mm) that the total root length was greater with small aggregates. Morphology of roots was also affected. Logsdon, Parker and Reneau (1987) observed significantly increase in root diameters within coarser aggregates. This effect of aggregate size on root growth could be due to an increase in mechanical resistance adjacent to the soil-root interface with increasing aggregate size (Misra, Alston and Dexter, 1986b,c), whereas the smaller aggregates did not impede root growth and may be displaced radially by roots more easily (Whiteley and Dexter, 1984; Logsdon, Parker and Reneau, 1987).

2.9 Compression of soil around roots

Roots affect the surrounding soil in many aspects. The pressure exerted by growing roots compresses the soil in their vicinity and locally changes the soil porosity and bulk density (Greacen and Sands, 1980). Many theoretical studies have been made

to model the deformation of soil around a growing root (e.g. Farrell and Greacen, 1966; Dexter, 1987; Becher, 1994; Kirby and Bengough, 2002). Farrell and Greacen (1966) employed the cavity expansion theory to describe the deformation of soil around roots. The model developped by Dexter (1987) predicts that the density decreases exponentially with distance from the roots surface. More recently, Becher (1994) showed that an expanding root compacts the adjacent soil and that this compaction depends on the initial conditions of the soil as well as on the root size. Using critical state model and finite element method, Kirby and Bengough (2002) predicted the greatest stresses to be at the very tip of the root cap. The stresses decreases with increasing distance from the root apex, and with increasing distance from the root surface.

Localization of compaction in sandy loam soil adjacent to root channels was first observed by Barley (1954). Using a radiograph technique, it has been also found that the bulk densities at the surface of pea, wheat and maize roots increased by 12, 28 and 20 % respectiveley at 3 mm from the root (Braunack and Freebairn,1988. cited by Young, 1998). Cockroft, Barley and Greacen (1969) reported a 8.5 % decrease in voids ratio adjacent to pea radicles in clay soil. The increase in bulk density was also evaluated by radiation techniques around metal probes (Greacen, Farrell and Forrest, 1967; Bradford, Farrell and Larson, 1971). It has been shown that the density patterns depend on the probe size and the tip form. Moreover, similar effect of an expanding cylindrical rubber tube, which simulates a growing root, on the surrounding granular media was also observed by Evans (1970) and Richards and Greacen (1986). Generally, the variation in soil density at the root surface, and the distance from the root surface where the soil is compressed, depends on the root diameter and the compressibility of the soil (Bengough, 2003).

2.10 Conclusion

Bulk density and soil strength are two major soil physical factors affecting root growth. The ability of plant roots to grow inside the compacted zones is closely related to the mechanical impedance of the soil medium as well as the internal properties of roots. Plants with greater root diameter (dicots) usually penetrate the compacted soils better than those with smaller root diameter (moncots). As response to increasing mechanical impedance, roots become shorter, thicker and the rate of elongation becomes smaller.

Theoretical studies on root growth based on penetrometer probes usually assum that the soil is homogeneous. As a consequence, change in penetrometer diameter does not influence the penetration pressure since the penetration force is proportional to the cross section of the probe. However, penetration tests in uniformly compacted sieved soil show that the penetration pressure differs from the predicted theoretical value when the probe diameter approaches the soil grain size. These observations indicate that the soil microstructures give rise to the size dependence of the penetration pressure, which is not adequately described by the classical continuum theory lacking a characteristic length. To avoid these deficiencies, further research of the phenomena occurring at the root scale is needed taking into account the microstructural features of the soil.

Chapter 3

Strain gradient plasticity

3.1 Introduction

Conventional models assume that the material behaves as local continuum. This implies that the state variable in a single material point depends only on that particular point and is not influenced by the surrounding material. In reality, however, no material is ideally local. Such plastic models, based on the standard continuum theory, fail to provide an objective description of localized deformation since they possess no material length scale and the typical dimensions of length that appear are associated with the overall geometry of the domain under consideration (Aifantis, 1999).

To resolve this issues, the introduction of spatial or nonlocal interactions into the continuum framework is required, which is achieved by taking into consideration of either the gradient of a state variable or a nonlocal state variable. Recently, several models incorporating material length scales have been proposed. These models are based on higher-order or nonlocal continuum theories, which are necessary to explain and simulate the behavior of heterogeneous materials (materials with microstructure). These models can be classified into three groups

- *Micropolar models*, that enhance the kinematic description of deformation by an additional field of local rotations, which can depend on the rotations corresponding to the displacement field. They display the property that the Cauchy stress tensor is no longer symmetric and that the so called couple stress tensors are present, which are thermodynamically conjugate to curvature tensors. The latter are expressed in terms of the spatial gradient of a microrotation tensor (Mühlhaus and Vardoulakis, 1987; de Borst and Sluys, 1991; Tejchman and Wu, 1993);

- *Nonlocal models*, that define state variables in an average form over a representative finite volume of the body, whose size is a characteristic of the material, and the material length parameter determines how the value of the variable at a certain point is weighted (Bažant and Pijaudier Cabot, 1988), and

- *Strain gradient models*, that characterize the deformation at a material point not only by the conventional strain but also by the strain gradients. This is governed by additional differential equations giving rise to additional boundary conditions for higher-order variables (Aifantis, 1984, 1987; Vardoulakis and Aifantis, 1991). In this dissertation, only the strain gradient theory will be used.

This chapter presents the necessary theoretical background of the classical plasticity theory and the gradient plasticity theory.

3.2 Classical plasticity

The classical theory of plasticity can be viewed as an extension of the theory of elasticity to account for nonlinear material behavior including permanent deformation.

The constitutive laws are based on: 1) the decomposition of strain into elastic and plastic parts, 2) the existence of a yield surface in the space of principal stresses, 3) the accompanying plastic flow rule, and 4) the hardening law. We confine ourselves to time independent models.

3.2.1 Strain decomposition

The total strain ϵ_{ij} can be decomposed into reversible elastic strain ϵ^e_{ij} and irreversible plastic strain ϵ^p_{ij} as

$$\epsilon_{ij} = \epsilon^e_{ij} + \epsilon^p_{ij} \tag{3.1}$$

The elastic strain is determined traditionally using a generalized Hooke's Law, which is expressed as

$$\sigma_{ij} = C_{ijkl}\epsilon^e_{kl} \tag{3.2}$$

where C_{ijkl} represents the elastic stiffness tensor, which, for isotropic materials, is defined as

$$C_{ijkl} = \frac{E\nu}{(1-2\nu)(1+\nu)}\delta_{ij}\delta_{kl} + \frac{E}{(1+\nu)}(\delta_{ik}\delta_{jl} + \delta_{il}\delta_{jk}) \tag{3.3}$$

where E is the Young's modulus, ν is the Poisson's ratio and δ is the Kronecker delta.

The decomposition of the total strain can be thought of as an expression for the elastic strain, $\epsilon^e_{ij} = \epsilon_{ij} - \epsilon^p_{ij}$. The stress response is related to the elastic strain as follows

$$\sigma_{ij} = C_{ijkl}(\epsilon_{ij} - \epsilon^p_{ij}) \tag{3.4}$$

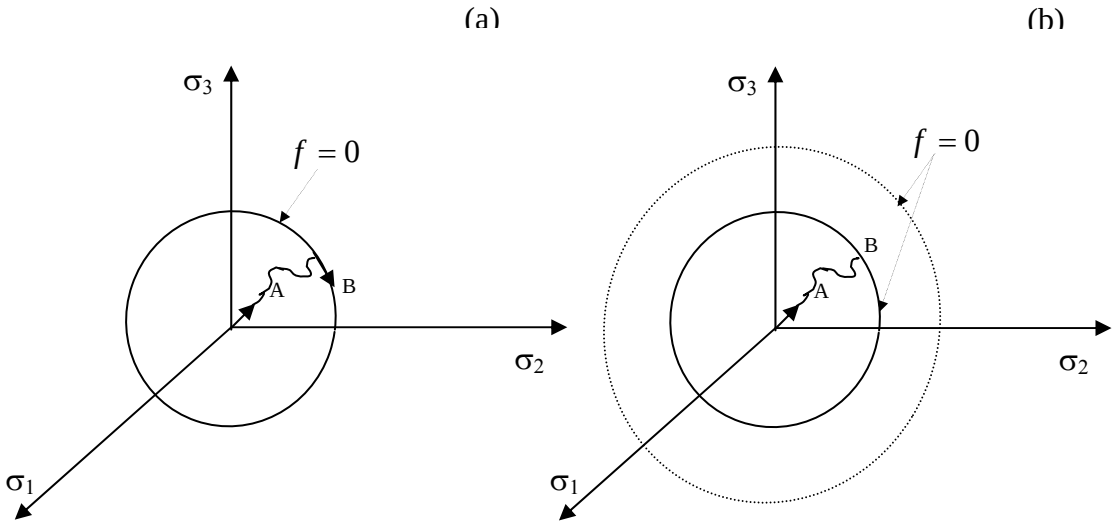

Figure 3.1: Evolution of the yield surface in the principal stress space for an elastic-perfectly plastic material (a) and for an elastoplastic hardenable material (b).

3.2.2 Yield criterion

In the space of principal stresses, there exists a yield surface, inside which the behavior is completely elastic. This surface is convex and depends on the stress variables, but can also depend upon other variables, k , often called hardening parameters. The yield surface is expressed through the following equation

$$f(\sigma_{ij}, k) = 0 \tag{3.5}$$

Plastic deformation can only occur when the stress state lies on the yield surface ($f > 0$ not admissible). In this case, if the yield surface does not change with stress history, the material is known as a perfectly plastic solid (Figure 3.1a). On the other hand, if the yield surface evolves during loading, an elastoplastic behavior with hardening is obtained (Figure 3.1b).

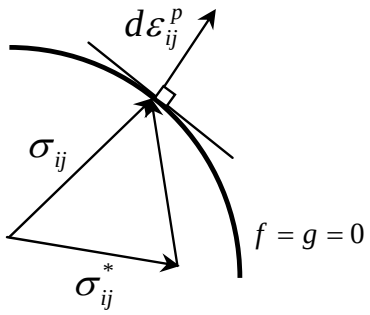

Figure 3.2: Principle of maximum plastic work

3.2.3 Flow rule

The general framework of thermodynamics postulates the existence of a plastic potential. The plastic potential, noted g, may also depend on the hardening parameters.

The flow rule is called associated, when the yield surface is coincident with the plastic potential ($f = g$). The direction of plastic strain vector in the space of principal strains is perpendicular to the yield surface. This leads to the following flow rule

$$d\epsilon_{ij}^{p} = d\lambda \frac{\partial f}{\partial \sigma_{ij}} \tag{3.6}$$

where $d\lambda$ is the plastic multiplier, which can be determined from the hardening law.

This type of material obeys the principle of maximum plastic work. This principle is reflected by the condition of normality of the plastic strain increment at any point on the boundary of the convex yield surface corresponding to the following inequality

$$(\sigma_{ij}^{*} - \sigma_{ij}) d\epsilon_{ij}^{p} \geq 0 \tag{3.7}$$

where σ_{ij} and σ_{ij}^{*} denote the stress tensors corresponding to two points, respectively, one inside the yield surface and the other on the yield surface (Figure 3.2).

The flow rule is called non-associated when the direction of plastic strain vector is perpendicular to the plastic potential $g(\sigma_{ij})$, which is distinct from the yield function $f(\sigma_{ij})$. The plastic flow rule then takes the form

$$d\epsilon_{ij}^{p} = d\lambda \frac{\partial g}{\partial \sigma_{ij}} \tag{3.8}$$

3.2.4 Hardening Laws

The hardening law governs the evolution of the yield surface in size, shape and/or location, with the loading history, in such a way that the current stress remains on the yield surface. This requirement is known as the the consistency condition, and is mathematically stated as

$$df(\sigma_{ij}, k) = 0 \tag{3.9}$$

Since the hardening parameter k is a function of the plastic strain, so the consistency condition can be written as follows

$$\frac{\partial f}{\partial \sigma_{ij}} d\sigma_{ij} + \frac{\partial f}{\partial k} \frac{\partial k}{\partial \epsilon_{ij}^{p}} d\epsilon_{ij}^{p} = 0 \tag{3.10}$$

Isotropic hardening represents a uniform expansion of the yield surface, independent of the direction of plastic flow. Classical kinematic hardening represents a translation of the locus of the yield surface, in stress space, in the direction of plastic flow. Mixed hardening is used when the two cases mentioned above are combined.

If the yield surface increases in size during loading, the material is said to be hardening. In contrast, softening is correspond to a decrease of the yield surface. Drucker's stability postulate, developed in the 1950s, defines the strain hardening materials as stable ($\sigma_{ij} d\epsilon_{ij}^{p} > 0$) and strain softening materials as unstable ($\sigma_{ij} d\epsilon_{ij}^{p} < 0$). The material behavior with $\sigma_{ij} d\epsilon_{ij}^{p} = 0$ are in elasticity or perfect plasticity.

3.2.5 General stress-strain relations

A general procedure for deriving a complete stress-strain relationship, according to the characteristics of plastic deformations, must be formulated in the incremental form. Equation (3.4) can be rewritten as

$$d\sigma_{ij} = C_{ijkl}(d\epsilon_{ij} - d\epsilon_{ij}^{P}) \tag{3.11}$$

Using the general non-associated plastic flow rule of equation (3.8) to express equation (3.11) in the following form

$$d\sigma_{ij} = C_{ijkl}\left(d\epsilon_{ij} - d\lambda\frac{\partial g}{\partial \sigma_{ij}}\right) \tag{3.12}$$

Substituting equation (3.12) into the consistency condition (3.10) gives

$$d\lambda = \frac{1}{H}\frac{\partial f}{\partial \sigma_{ij}}C_{ijkl}d\epsilon_{kl}^{p} \tag{3.13}$$

where H is given by

$$H = \frac{\partial f}{\partial \sigma_{ij}}C_{ijkl}\frac{\partial g}{\partial \sigma_{kl}} - \frac{\partial f}{\partial k}\frac{\partial k}{\partial \epsilon_{ij}^{p}}\frac{\partial g}{\partial \sigma_{ij}} \tag{3.14}$$

By substituting equation (3.13) into equation (3.12), the complete relation between the stress and strain increments is obtained as follows

$$d\sigma_{ij} = \left(C_{ijkl} - C_{ijkl}^{p}\right)d\epsilon_{kl} \tag{3.15}$$

where C_{ijkl}^{p} is the stiffness tensor of plastic behavior defined as

$$C_{ijkl}^{p} = \frac{1}{H}C_{ijmn}\frac{\partial g}{\partial \sigma_{mn}}\frac{\partial f}{\partial \sigma_{pq}}C_{pqkl} \tag{3.16}$$

The above procedure is valid for both isotropic strain hardening and perfectly plastic solids. For the case of perfectly plastic solids, equation (3.14) takes the following form

$$H = \frac{\partial f}{\partial \sigma_{ij}}C_{ijkl}\frac{\partial g}{\partial \sigma_{kl}} \tag{3.17}$$

3.2.6 Plasticity models

Plasticity models are defined by a yield or failure criterion characterizing the strength properties of the material. The yield criterion limits the elastic domain during loading, whereas the failure criterion gives the maximum deviatoric stress that can be applied. There are a number of models proposed for different materials. Some of the commonly used yield or failure criteria are the Tresca and Von Mises yield criteria, which are independent of the hydrostatic stress and, the pressure sensitive yield criteria, i.e. Mohr-Coulomb and Drucker-Prager yield criteria, which incorporate the effect of the hydrostatic pressure on the yield surface (see Yu, 2006 and Nakai, 2013).

Tresca criterion

According to the Tresca yield criterion (1864), yielding of a material begins when the maximum shear stress at a point reaches a critical value k. If σ_1, σ_2 and σ_3 are the principal stresses, the Tresca criterion can be expressed as

$$Max\left\{\left|\sigma_1-\sigma_2\right|,\left|\sigma_2-\sigma_3\right|,\left|\sigma_3-\sigma_1\right|\right\}=2k \tag{3.18}$$

where k is a material parameter determined experimentally by a tension test.

In the principal stress space, the yield surface is a prism parallel to the hydrostatic axis ($\sigma_1=\sigma_2=\sigma_3$)(Figure 3.3a). The section on the deviatoric plane is a regular hexagon (Figure 3.3b).

Von Mises criterion

In the Von Mises criterion, yielding occurrs when the second invariant of deviatoric stress, $J_2=s_{ij}s_{ij}/2$, reaches a critical value. Von Mises yield criterion is expressed

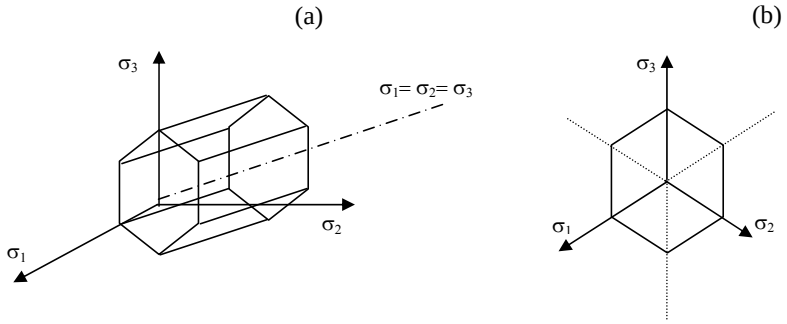

Figure 3.3: Tresca yield surface a) in the principal stress space; b) in the deviatoric plane.

as follows

$$\sqrt{J_2} - k = 0 \tag{3.19}$$

or

$$(\sigma_1 - \sigma_2)^2 + (\sigma_2 - \sigma_3)^2 + (\sigma_3 - \sigma_1)^2 - 6k^2 = 0 \tag{3.20}$$

where k is a material parameter. Alternatively the criterion ca be expressed directly in terms of the effective stress as

$$\sigma_e - k = 0 \tag{3.21}$$

where $\sigma_e = \sqrt{\frac{2}{3} s_{ij} s_{ij}}$ is the effective stress and $s_{ij} = \sigma_{ij} - \frac{1}{3}\sigma_{kk}\delta_{ij}$ is the deviatoric stress tensor. The physical explanation of Von Mises yield criterion is that yielding begins when the elastic energy of distortion reaches a critical value (Hill, 1950).

Geometrically, Von Mises yield criterion represents a right circular cylinder, whose generator is equally inclined to the principal stress axes (Figure 3.4a). The section on the deviatoric plane is a circle (Figure 3.4b).

Mohr-Coulomb yield criterion

According to the Mohr-Coulomb criterion, yielding is assumed to occur when the shear stress, τ, on any plane reaches a value that depends linearly on the normal

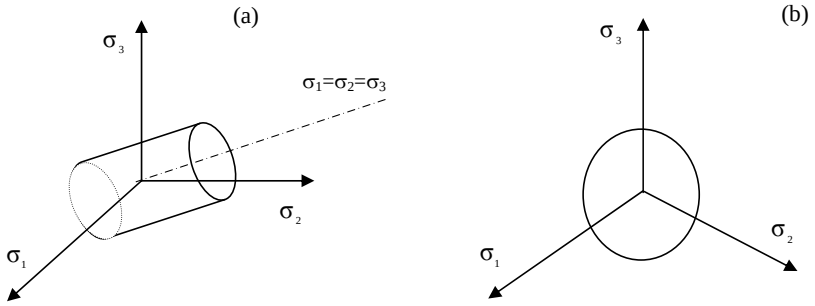

Figure 3.4: Von Mises yield surface a) in the principal stress space; b) in the deviatoric plane.

stress, σ_n, on the same plane (see Sec. 2.3).

In term of the principal stresses (for $\sigma_1 \geq \sigma_2 \geq \sigma_3$), the Mohr-Coulomb yield criterion can be expressed by

$$\sigma_1 - \sigma_3 - (\sigma_1 - \sigma_3)\sin\varphi - 2c\cos\varphi = 0 \tag{3.22}$$

where c and φ are respectively the cohesion and the friction angle of the material. In the special case of frictionless materials, for which $\varphi = 0$, equation (3.22) reduces to the maximum shear stress criterion of Tresca.

Drucker-Prager yield criterion

The Drucker-Prager criterion, formulated in 1952, is a smooth approximation of the Mohr-Coulomb criterion (Figure 3.4) and is an extension of the Von Mises criterion, where the influence of the hydrostatic component on failure is introduced by inclusion of an additional term in the Von Mises expression to give

$$\sqrt{J_2} + \mu I_1 - k = 0 \tag{3.23}$$

where $I_1 = \sigma_{ii}$ is the first invariant of stress tensor, μ and k are material parameter. When μ is zero, equation (3.23) reduces to the Von Mises criterion.

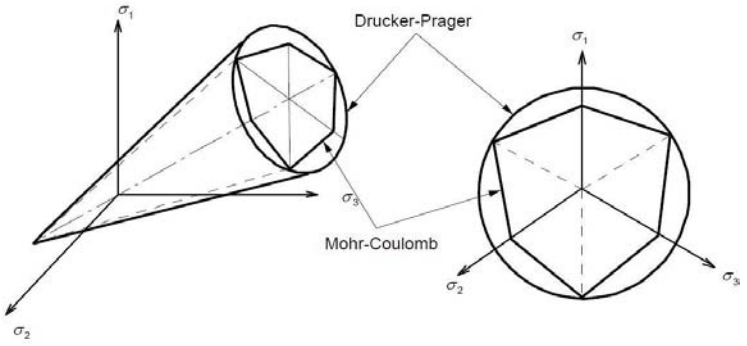

Figure 3.5: Mohr-Coulomb and Drucker-Prager yield criteria.

3.3 Gradient plasticity

Conventional continuum theories assume that stress at a material point is a function of state variables, such as strain, at the same point. Although this local assumption has long been proved for homogeneous deformation and stress fields, it is inappropriate when the material behavior at this point is influenced by the deformation of neighboring points. Under these circumstances, standard continuum models fail to predict the actual material behavior. Not only do to their inability to predict the influence of the microstructures on the global mechanical behavior of the material, but they also suffer from mathematical difficulties for localized deformation and cannot account for scale effects. These effects can be successfully captured by continuum theories that include a material length scale, which is closely related to the microscopical structures such as the mean grain diameter in granular materials (Vardoulakis and Aifantis, 1989).

The strain gradient plasticity has been formulated to account for length scale-dependence in plasticity. It was intended primarily to solve problems related to localization, mesh dependence in certain FE-simulations and to estimate the width and spacing of shear bands. The basic idea of the gradient plasticity was first initiated by Aifantis (1984) to describe the width of shear bands in metals. He

assumed that the yield function of the material is related to the strain gradient in such way that an additional material length scale can be introduced while leaving the other features of plasticity theory unchanged.

In an analysis of shear bands of a class of ductile materials with rate independent response, Coleman and Hodgdon (1985) presented an analytical solution of a one dimensional non-linear constitutive model with strain gradient. They proposed a direct gradient modification of the flow rule through the use of the consistency condition. They included a term that accounts for the spatial derivative of the accumulated shear strain in the evaluation of the stress field, which becomes the Laplacian of the accumulated distortion in the three dimensional generalization.

Schreyer and Chen (1986) used a gradient constitutive model in a one dimensional problem to study the relationship between material softening and structural softening. They proposed a gradient model in which the current yield stress depends on both the plastic strain and its first spatial gradient.

Vardoulakis and Aifantis (1989; 1991) extended the gradient plasticity model for frictional/dilatent materials by incorporating the second order strain gradients into the flow rule, yield condition, and/or dilatancy condition. The extra boundary conditions associated with the gradient term are obtained using the principle of virtual work. A complete description of the Aifantis gradient plasticity in connection with shear band analysis is provided in Mühlhaus and Aifantis (1991). The authors presented a variational formulation that incorporates the Laplacian of the plastic consistency parameter in such way that the same interpolation functions for both the displacements and the plastic parameter are obtained. Extra boundary conditions are then needed for the plastic strain fields.

A general formulation and a solution algorithm for the gradient dependent plasticity, in a finite element context, have been presented by de Borst and Mühlhaus

(1992). They presented a mixed formulation with the displacement and the effective plastic strain treated as nodal unknowns to simulate the strain softening behavior. Their formulations and algorithms are able to solve two or three dimensional boundary value problems. The same framework has been used by de Borst and Pamin (1996) in a 2D finite element formulation. Numerical results of plane strain compression illustrates stability after localization and insensitivity to mesh refinement and alignment for the gradient theory. Recently, the gradient theory was also implemented into meshless methods by Chen, Wu and Belytschko (2000) and finite difference method by Alehossein and Korinets (2000). Furthermore, Peerlings et *al.*, (1998) extended gradient theory to construct a gradient-enhanced damage model for concrete. Drawing from this inspiration, an implicit gradient model for metal plasticity has been also developed by Engelen, Geers and Baajens (2003). The authors postulate the dependence of the yield stress on the hardening variable and an additional quantity, which can be interpreted as a nonlocal hardening variable and showed numerical simulations with a gradient formulation.

3.3.1 Aifantis' theory

The simplest form of the strain gradient theory, proposed by Aifantis in the early 1980s, is based on the introduction of the Laplacian of the effective strain ϵ_p into the constitutive expression for the flow stress $\bar{\sigma}$. In his model Aifantis assumes that the actual flow stress is linearly related to the gradient of the equivalent plastic strain in the form

$$\bar{\sigma}(\epsilon_p, \nabla^2\epsilon_p) = \bar{\sigma}(\epsilon_p) - c\nabla^2\epsilon_p \tag{3.24}$$

The corresponding form of the yield function can be written as

$$f(\bar{\sigma}(\epsilon_p, \nabla^2\epsilon_p)) = f(\bar{\sigma}(\epsilon_p)) - c\nabla^2\epsilon_p \tag{3.25}$$

where $f(\bar{\sigma}(\epsilon_p))$ is an expression of the flow stress from the classic (or local) model, $\epsilon_p = \sqrt{2\epsilon_{ij}\epsilon_{ij}/3}$ is the equivalent plastic strain, c is a material parameter with the dimension of force, which may be calibrated through shear band thickness measurements (Zbib and Aifantis, 1992), and the definition

$$\nabla^2 = \frac{\partial^2}{\partial r^2} + \frac{1}{r}\frac{\partial}{\partial r} + \frac{1}{r^2}\frac{\partial^2}{\partial \theta^2} \tag{3.26}$$

for the laplacian operator in polar coordinates.

By making use of the gradient dependence of the yield function in (3.25), the plastic consistency condition $\dot{f} = 0$ becomes the following differential equation

$$\frac{\partial f}{\partial \sigma}\dot{\sigma} + \frac{\partial f}{\partial \epsilon_p}\dot{\epsilon}_p + \frac{\partial f}{\partial \nabla^2 \epsilon_p}\nabla^2\dot{\epsilon}_p = 0 \tag{3.27}$$

According to the classical flow theory, the plastic multiplier defined in (3.6) can be written as

$$\dot{\epsilon}^p = \dot{\lambda} n \tag{3.28}$$

where n is the plastic flow direction tensor. The consistency condition takes then the form (de Borst and Mülhaus, 1992)

$$n\dot{\sigma} + \frac{\partial f}{\partial \lambda}\dot{\lambda} \; + \frac{\partial f}{\partial \nabla^2 \lambda}\nabla^2\dot{\lambda} = 0 \tag{3.29}$$

The resulting equation is a differential equation for λ unlike conventional plasticity where the plastic multiplier can be determined locally from an algebraic equation. The dependence of the yield function on the second order derivatives of the effective plastic strain requires non-standard boundary conditions. Mühlhaus and Aifantis (1991) assumed,with the help of the variational principle, appropriate boundary conditions for the plastic multiplier ($\nabla\dot{\lambda} = 0$) at the elastic-plastic interface. By solving the equation (3.29) together with the incremental equilibrium equation, the gradient plasticity theory is capable of describing the plastic behavior of materials and capturing the heterogeneity and size effects.

3.3.2 Strain gradient plasticity interpretation of size effects

The problem of size effect has been investigated by several researchers using gradient plasticity theory (Zhu, Zbib and Aifantis, 1997; Aifantis, 1999). By introducing the strain gradients into the constitutive equation, a material length scale is included into plasticity theory, providing a framework for modeling phenomena with length scales. As described by Fleck et al. (1994) there are two different size effects of plastic deformations. The first group is the dependence of material behavior on the size of the volume under consideration when the material and geometry shape are kept unchanged. For example, the indentation hardness increases as the thickness of films is decreased (Nix, 1989). The second category is due to the size and arrangement of microstructure for example the Hall-Petch hardening effect. This is due to the fact that the flow stress of a polycrystal is inversely proportional to the square root of the grain size.

For interpreting size effects in metal matrix composites, Zhu, Zbib and Aifantis (1997) solved a boundary value problem by FEM. Comparison between the proposed model predictions and experimental data shows that the strength of metal matrix composites decreases with increasing particle size of reinforcement for all materials studied. For soils and concrete, the size effect was discussed by Vardoulakis and Sulem (1995) and Harris and Sabnis (1999).

Size effects have been also observed for hardening materials on millimeter and micrometer scales, e.g. bending of thin beams (Stölken and Evans, 1998), torsion of thin wires (Fleck et al., 1994) and micro indentation (Nix, 1989). The results of these experiments cannot be described by standard plasticity theories since their constitutive models possess no material length scale.

Bending of thin beams

A micro bending test for thin foils was presented by Stölken and Evans (1998). In their experiments, nickel foils of different thicknesses were subjected to bending. The deformed radius of curvature of an elastically unloaded foil was measured. The authors observed an increase in normalized moment for decreasing foil thickness from 50 μm to 12 μ, which give improved currency of the notion of a size effect for plasticity at small scales.

Richards (1958) tested beams of mild steel to investigate size effect on yielding in pure bending. The beams were in five different sizes, which were geometrically similar. He observed that the value of yield initiation increases significantly as the specimen size is decreased from the largest to the smallest. Aifantis (1999) showed that this effect can be described using strain gradient plasticity theory. Due to $\nabla^2\epsilon = 0$ in the case of pure bending, he adopted a gradient dependent stress-strain relation using first and second gradients in the form

$$\bar{\sigma} = \sigma_0 - c_1 \left|\nabla\epsilon_p\right| - c_2\nabla^2\epsilon_p \tag{3.30}$$

where $(\bar{\sigma}, \epsilon_p)$ denote the equivalent stress and strain, σ_0 is the tensile yield stress and (c_1, c_2) are the gradient coefficients. The rest of the model (strain distribution, Hooke's law for the elastic strains etc.) is kept unchanged as in the classical continuum theory.

Let κ be the curvature of the beam and h its thickness. The axial stress and the axial strain in the elastic region are given by $\sigma = E\epsilon$ and $\epsilon = \kappa y$ respectively, where E is the Young's modulus and y is the coordinate along the depth of the beam, measured from the neutral axis.

Using the same relationship of the stress and stain for the equivalent stress and equivalent strain, Aifantis (1999) assumed that yielding first occurs when the stress

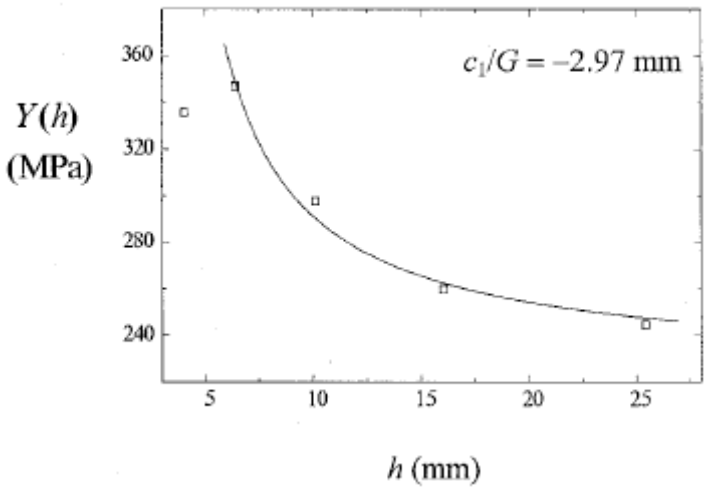

Figure 3.6: comparison between theory and experiment in yielding behavior in pure bending (Aifantis, 1999)

at the outer surface of the beam becomes equal to the yield stress value Y then

$$Y = E\kappa h/2 = \sigma_0 - c_1\kappa \tag{3.31}$$

The expression for the dependence of the yield stress Y at the outer surface of the beam on the height h of its cross-section is therefore obtained as, which is plotted in Figure 3.6

$$Y = \sigma_0 \left(\frac{h/2}{(h/2) + (c_1/E)} \right) \tag{3.32}$$

Torsion of thin wires

Fleck et al. (1994) observed in micro-torsion of thin copper wires that the scaled shear strength increases by a factor of 3 as the wire diameter decreases from 170 to 12 μm. In order to fit their experimental data, Aifantis (2003) employed the gradient-dependent flow stress given by

$$\tau = \kappa(\epsilon_p) + c_1(\epsilon_p) \left|\nabla\epsilon_p\right|^2 + c_2(\epsilon_p)\nabla^2\epsilon_p \tag{3.33}$$

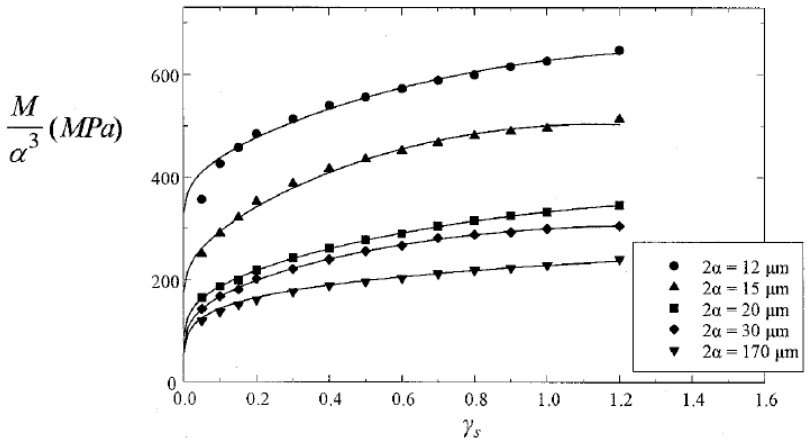

Figure 3.7: Comparison between theory and experiment for twisted Cu wires (Aifantis, 2003)

A power law expression is assumed for the homogeneous part of the flow stress and a similar relation is adopted for the gradient coefficients ($\kappa(\epsilon_p) = \kappa_0 \epsilon_p^n$, $c_1 = (1/2)(dc_2/d\epsilon_p)$ and $c_2 = c\epsilon_p^{n-1}$). The size dependent twisting moment M vs. the surface shear strain of the wire γ_s ($\gamma_s = \varphi\alpha$) is expressed as

$$\frac{M}{\alpha^3} = 2\pi \left(\frac{\kappa_0}{n+3} + \frac{c}{2\alpha^2} \right) \gamma_s^n \tag{3.34}$$

with φ denoting the angle of twist per unit length and α the wire radius. Figure 3.7 shows the fitting of experimental results obtained by Aifantis (2003) for the size dependence for the twisting moment M.

3.3.3 Length scale and strain localization

Strain localization in granular materials has been extensively investigated by many researchers. Experimental, theoretical and numerical studies in this area show that the deformation is localized within a confined region, called shear band, where its thickness is finite and related to the heterogeneous material microstructure (Pamin and de Borst, 1995). Roscoe (1970) observed the localization phenomenon in dif-

ferent soils using model tests and the centrifuge technique. Using X-ray techniques, he showed that the shear band thickness was 8 - 10 times the mean grain diameter. The same technique was used by Vardoulakis and Graf (1985) to measure the shear band thickness in fine and medium grained sand specimens tested under plane-strain conditions. The thickness was found about 16 times the mean grain diameter of the soil. Other techniques have also been used such as stereophotographic techniques (Desrues, Lanier and Stutz, 1985), Laser techniques (Tatsuoka et al. 1990), Tomography (Desrues et al., 1996).

The localization of plastic deformation into a shear band was discussed by Rudnicki and Rice (1975) and Rice (1976). They treated shear band formulation as material instabilities by bifurcation theory. They analyzed the emergence and inclination of the shear band but they did not consider its thickness since their constitutive theory does not include any length. Aifantis (1984; 1987) and Zbib and Aifantis (1988) introduced an internal length scale by including strain gradients into the yield condition of plasticity. Based on the same theory, Vardoulakis and Aifantis (1991) obtained the expression for the thickness of shear band by adding second order strain gradients into the flow rule and the yield condition. In addition to the emergence and inclination of the localized zones, the gradient approach is shown to be able to capture the shear band thickness and the post localization behavior.

The need of strain gradient plasticity originates from the inability of the classical plasticity models to describe the localization of plastic deformation because the conventional models possess no material length scales. Within the frame of classical constitutive theories the numerical simulation of localization exhibit a pathological mesh-dependency and high sensitivity to constitutive relations (de Borst and Pamin, 1996). Mathematically, the mesh dependence is a direct consequence of the fact that the solution is not unique and the size of the localization zones is therefore

defined by the spacing of the discretization (Pamin, 1994). In contrast, due to the introduction of gradient terms, the aforementioned mathematical difficulties are removed and therefore, the appropriate differential equations for the deformation are able to estimate the shear band thickness and spacings.

3.3.4 Conclusion

As a generalization of the classical plasticity theory, strain gradient theory enriches the classical continuum with additional material length scales to account for the underlining microstructure of the material. Through this length scale, size effects or localized plastic deformation that are not captured or explained by standard theories, can be modeled properly through the introduction of higher order spatial gradients of strain or internal variables.

Strain gradient plasticity formulations have been developed to avoid false solution for the localization and excessive mesh dependence, and to describe the experimentally observed size effects such as the effect of wire thickness on torsional response, the dependence of the initial low stress upon sample size and the dependence of hardness on size of the indenter. Strain gradient theory presents a promising approach to model the scale effect observed in the growth of plant roots.

Chapter 4

Cavity Expansion

4.1 Introduction

The problem of cavity expansion in finite or infinite media has attracted much attention from researchers in both mechanics and material science. Its theoretical appeal has always been the simplicity of its geometry, which has made it possible to obtain relatively simple solutions in a number of different materials including metals, plastics, rocks and soils.

The cavity expansion theory was first developed for applications to metal indentations problems (Bishop et al., 1945; Hill, 1950). Its application to geotechnical problems came later (e.g. Gibson and Anderson, 1961; Meyerhof, 1951). The analysis of cylindrical and spherical cavity expansions has been widely applied to practical problems such as the interpretations of pressuremeter tests (Gibson and Anderson, 1961; Vesic, 1972; Palmer, 1972; Houlsby and Withers, 1988; Yu, 1990), the installation of driven piles (e.g. Randolph, Carter and Wrath, 1979), cone penetration tests (e.g. Salgado, Mitchell and Jamiolkowski, 1997; Cudmani and Osinov, 2001) and the bearing capacity of deep foundations (Vesic, 1977; Randolph et al., 1979). Cavity expansion solutions not only provide valuable predictions for the deformation

and pressure-expansion behavior of these applications, but also furnish benchmarks for comparison with experimental data.

Existing studies in this area vary because of differences in the constitutive models for the stress-strain behavior of the expanding body. Most analyses are mainly restricted to elastic-perfectly plastic solid. Hill (1950) gave a general solution of the finite expansion of the spherical cavity in a Tresca material. Chadwick (1959) presented the solution for an elastic-plastic material with Mohr-Coulomb yield surface obeying the associated flow rule. In both cases the solution were obtained with the assumption of small deformations and incompressibility of the material in the plastic zone. Vesic (1972) studied spherical and cylindrical cavities in both cohesive and frictional soils. He adopted Mohr-Coulomb yield surface with non-associated flow rule, and suggested a procedure to account for the volume change in the plastic region.

Carter, Booker and Yeung (1986) presented an analytical solution for the limit pressure in a non-associated Mohr-Coulomb material. Yu and Houlsby (1991) extended this theory by introducing large strains in the plastic region, whereas the elastic region is treated by a small-strain approach. The limit pressure was obtained as a function of the dilatancy angle, friction angle, elastic moduli and initial stress state.

Collins and Yu, (1996) provided an analytical study of the large strain undrained expansion of cylindrical and spherical cavities with critical-state soil models. The sand response was governed by a state parameter, which depends on the current void ratio and the current mean stress. The expansion of cavity was considered from zero initial radius. Durban and Fleck (1997) presented a finite strain analysis for spherical cavity in a Drucker-Prager material. The material was modeled by a non-associated deformation theory with arbitrary strain-hardening.

Essential to the previous theoretical developments is that the constitutive response of the materials is described by conventional continuum theory for homogeneously deforming media. Thus, they do not include internal length scale, and unable to model the influence of microstructure since the governing equations can be written in a dimensionless form, predicting for all geometrically similar cavities the same limit pressure. To resolve this problem, high-order term must be introduced into the classical plasticity theory. This extension implicates additional material parameter, which takes the microstructure of the soil into consideration and therefore, the observed size dependence can be properly modeled.

To investigate the size effects in a cylindrical and spherical cavities subjected to internal pressure, Gao (2003a, b) developed an analytical solutions of the cavity expansion problem using strain gradient plasticity theory with power-law hardening and von-Mises yield criterion. The stress components were obtained as a function of the inner radius of the cavity. Similar size dependence behavior was studied by Tsagrakis et al. (2006) for internally pressurized thick-walled hollow cylinder using both deformation and flow theories. Zhao, Sheng and Sloan (2007) presented a numerical analysis on expanded cylindrical cavity using Tresca criterion to describe the yield behavior. More recently, Zhao (2011) extended his solution to account for a special class of cohesive-frictional micromorphic media using the Mohr-Coulomb yield criterion. Gao, Park and Ma (2009) and Collin, Caillerie and Chambon (2009) have been limited their solutions of cavity expansion problems using gradient elasticity only.

In this chapter, analytical solutions for the expansion of spherical cavity subjected to internal and external pressures are presented. The associated Drucker-Prager yield criterion is extended to include higher-order strain gradients. Explicit expressions for the stresses, strain and displacements are derived similar to the the

work of Gao (2003b).

4.2 Cavity expansion in cohesive-frictional soils

To begin with the development of the gradient dependent constitutive model, recall the yield function and the plastic potential for the Drucker-Prager model

$$f = \sqrt{J_2} + \mu I_1 - \bar{\sigma} \tag{4.1}$$

$$g = \sqrt{J_2} + \mu_\psi I_1 \tag{4.2}$$

where $I_1 = \sigma_{ii}$ is the first invariant of stress tensor, $J_2 = \frac{1}{2} S_{ij} S_{ij}$ is the second invariant of the deviatoric stress $S_{ij} = \sigma_{ij} - \frac{1}{3}\sigma_{ii}\delta_{ij}$, $\bar{\sigma}$ is the flow stress, μ is the friction coefficient and μ_ψ is the dilatation factor. Acossiated plasticity is recovered for $\mu_\psi = \mu$ and the von Mises model is obtained with $\mu_\psi = \mu = 0$. The flow stress $\bar{\sigma}$ is assumed to depend on the higher order strain gradient in the following manner

$$\bar{\sigma} = \bar{\sigma}(\epsilon_p) - c\nabla^2 \epsilon_p \tag{4.3}$$

where $\epsilon_p = \sqrt{2\epsilon_{ij}\epsilon_{ij}/3}$ is the effective plastic strain and c is a gradient-related coefficient. The above formulation represents the simplest version of gradient theory by introducing the higher order term into the yield function while leaving the other features of plasticity theory unchanged.

Problem formulation

Consider a thick walled spherical cavity of inner radius a and outer radius b subjected to a uniform pressure p_0 on external surface and p on the internal surface (Figure 4.1). Since both the geometry and the load are axisymmetric, all field variables depend only on the radial displacement u.

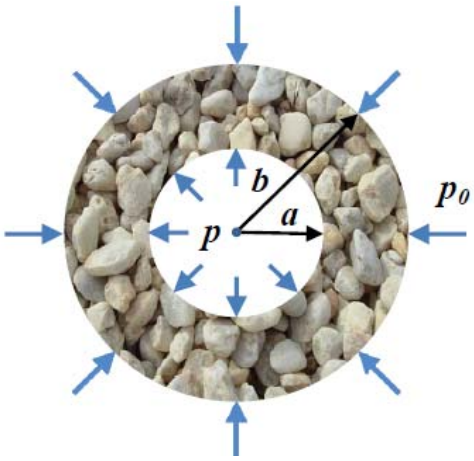

Figure 4.1: Cavity expansion problem

Initially ($t = 0$) the cavity has an internal and external radii a_0 and b_0 and a internal pressure p_0. At time t the cavity pressure is increased to p and the cavity radii increased to a and b respectively.

Considering an element at a radial distance r from the cavity center, the equation of equilibrium can be expressed as follows

$$2(\sigma_\theta - \sigma_r) = r\frac{d\sigma_r}{dr} \tag{4.4}$$

where σ_r and σ_θ are normal stresses in the radial and tangential directions respectively. The radial stress is known on both internal and external boundaries. These boundary conditions can be written as:

$$\begin{aligned} \sigma_r|_{r=a} &= -p \\ \sigma_r|_{r=b} &= -p_0 \end{aligned} \tag{4.5}$$

Under infinitesimal deformation, the three nonzero strain components can be written out readily

$$\begin{aligned} \epsilon_r &= \frac{du}{dr} \\ \epsilon_\theta &= \epsilon_\varphi = \frac{u}{r} \end{aligned} \tag{4.6}$$

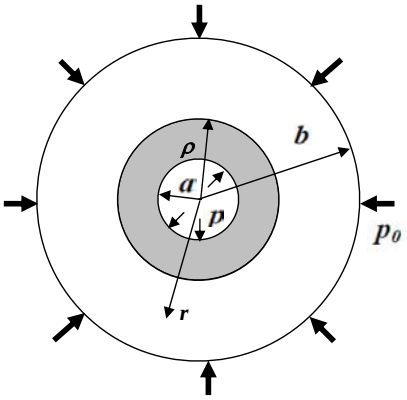

Figure 4.2: Cavity during expansion

Equation (4.6) can be used to eliminate the displacement u to give the following compatibility condition

$$\epsilon_r - \epsilon_\theta = r\frac{d\epsilon_\theta}{dr} \tag{4.7}$$

If p_0 is sufficiently small, the deformation of soil is purely elastic. Along with increasing to p, a plastic zone around the cavity will develop. The radial distance of the plastic zone around the cavity is denoted by ρ. The soil beyond the plastic zone remains in a state of elastic equilibrium. The property of the soil in the elastic zone is defined by Young's modulus, E, and Poisson ratio, ν. The soil is assumed to obey Hookian elasticity until the onset of yield. Yielding of the soil is described by the Drucker-Prager model. The elastic and plastic regions of the soil are separately considered.

Elastic solution

As the cavity pressure increases from its initial value, the deformation of the soil is at first purely elastic. The elastic region can be considered as an elastic thick-walled hollow sphere of the inner radius ρ and outer radius b, subjected to a uniform internal pressure $p_\rho = p(\rho)$. Under conditions of radial symmetry the elastic stress-strain

relationship may be expressed as:

$$\begin{aligned} \epsilon_r &= \frac{1}{E}\left(\sigma_r - 2\sigma_\theta\right) \\ \epsilon_\theta &= \epsilon_\varphi = \frac{1}{E}\left(-\nu\sigma_r + (1-\nu)\sigma_\theta\right) \end{aligned} \tag{4.8}$$

The stress and the radial displacement distributions can be expressed as follows (Yu, 2000)

$$\sigma_r = -p_0 + (p_\rho - p_0)\left(\frac{1}{(b/\rho)^3 - 1} - \frac{1}{(r/\rho)^3 - (r/b)^3}\right) \tag{4.9}$$

$$\sigma_\theta = -p_0 + (p_\rho - p_0)\left(\frac{1}{(b/\rho)^3 - 1} + \frac{1/2}{(r/\rho)^3 - (r/b)^3}\right) \tag{4.10}$$

$$u = r - r_0 = \frac{p_\rho - p_0}{2G(1/\rho^3 - 1/b^3)}\left(\frac{1-2\nu}{(1+\nu)b^3}r + \frac{1}{2r^2}\right) \tag{4.11}$$

where $G = E/2(1+\nu)$ is the shear modulus of the material. The corresponding expressions for the non-vanishing strain distributions can be easily obtained from (4.11) and (4.6).

In the above expressions for stress, strain and displacement distributions, two unknown parameters p_ρ and ρ, are needed to be determined in term of the applied pressure p using the continuity of the stresses and displacements at the elastic-plastic interface.

Plastic solution

After the initial yielding at the cavity wall, a zone of soil extending from the cavity wall to a radial distance ρ becomes plastic as the cavity pressure continues to increase. The boundary-value problem for determining the stress and strain components in the plastic zone can be solved analytically by considering the equilibrium equation, the constitutive equations, and the boundary conditions.

The Drucker-Prager yield surface is defined for the spherical cavity as

$$f = \sigma_\theta - \sigma_r + \frac{1}{3}\mu\left(\sigma_r + 2\sigma_\theta\right) - \bar{\sigma} \tag{4.12}$$

Assuming a power hardening low for the flow stress $\bar{\sigma}$, the gradient-dependent form of equation (4.3) can be written as

$$\bar{\sigma} = \kappa\epsilon_p^m - c\nabla^2\epsilon_p \tag{4.13}$$

where κ and m are material parameters.

Within the plastic zone, the constitutive equations, with associated flow rule are given by (Durban and Fleck, 1997)

$$\begin{aligned} \epsilon_r &= \left(-1 + \frac{1}{3}\mu\right)\epsilon_p \\ \epsilon_\theta &= \epsilon_\varphi = \left(\frac{1}{3} + \frac{1}{3}\mu\right)\epsilon_p \end{aligned} \tag{4.14}$$

Substituting equations (4.14) into equation (4.7) yields

$$\frac{d\epsilon_p}{\epsilon_p} = \frac{-9}{3+2\mu}\frac{dr}{r} \tag{4.15}$$

The gradient term in the constitutive equation needs additional boundary conditions for the equivalent plastic strain in the following form

$$\epsilon_p|_{r=a} = \epsilon_{pa} \tag{4.16}$$

$$\epsilon_p|_{r=\rho} = \frac{\sigma_y}{E} \tag{4.17}$$

where σ_y is the yield stress and ϵ_{pa} is a constant to be determined as a part of the solution.

The solution procedure starts with integrating (4.15) from a to r and after applying the appropriate boundary condition at the cavity wall, the effective strain is obtained as

$$\epsilon_p = \epsilon_{pa}\left(\frac{a}{r}\right)^{\frac{9}{3+2\mu}} \tag{4.18}$$

By making use of equation (4.18) into equation (4.17) gives

$$\epsilon_{pa} = \frac{\sigma_y}{E}\left(\frac{\rho}{a}\right)^{\frac{9}{3+2\mu}} \tag{4.19}$$

Introducing equation (4.18), equation (4.13) becomes

$$\bar{\sigma} = \kappa\epsilon_{pa}^{m}\left(\frac{a}{r}\right)^{\frac{9m}{3+2\mu}} - c\frac{9(6-2\mu)\epsilon_{pa}}{(3+2\mu)^2}\frac{1}{a^2}\left(\frac{a}{r}\right)^{\frac{15+4\mu}{3+2\mu}} \tag{4.20}$$

Substituting equations (4.20) and (4.12) into equation (4.4) gives

$$d\sigma_r = 2\left(\frac{3\kappa\epsilon_{pa}^{m}}{3+2\mu}\frac{1}{r}\left(\frac{a}{r}\right)^{\frac{9m}{3+2\mu}} - \frac{3\mu}{3+2\mu}\frac{1}{r}\sigma_r - c\frac{27(6-2\mu)\epsilon_{pa}}{(3+2\mu)^3}\frac{1}{a^2}\frac{1}{r}\left(\frac{a}{r}\right)^{\frac{15+4\mu}{3+2\mu}}\right)dr \tag{4.21}$$

After some algebraic manipulations, the desired differential equation is obtained as

$$d\left(\sigma_r r^{\frac{6\mu}{3+2\mu}}\right) = 2r^{\frac{6\mu}{3+2\mu}}\left(\frac{3\kappa\epsilon_{pa}^{m}}{3+2\mu}\frac{1}{r}\left(\frac{a}{r}\right)^{\frac{9m}{3+2\mu}} - c\frac{27(6-2\mu)\epsilon_{pa}}{(3+2\mu)^3}\frac{1}{a^2}\left(\frac{a}{r}\right)^{\frac{15+4\mu}{3+2\mu}}\right)dr \tag{4.22}$$

A direct integration of the resulting differential equation (4.22) from a to r leads to

$$\begin{aligned}\sigma_r &= -p\left(\frac{a}{r}\right)^{\frac{6\mu}{3+2\mu}} + 2\frac{\kappa\epsilon_{pa}^{m}}{3m-2\mu}\left(\left(\frac{a}{r}\right)^{\frac{6\mu}{3+2\mu}} - \left(\frac{a}{r}\right)^{\frac{9m}{3+2\mu}}\right)\\ &\quad -2c\frac{27(6-2\mu)\epsilon_{pa}}{(3+2\mu)^2(15-2\mu)}\frac{1}{a^2}\left(\left(\frac{a}{r}\right)^{\frac{6\mu}{3+2\mu}} - \left(\frac{a}{r}\right)^{\frac{15+4\mu}{3+2\mu}}\right)\end{aligned} \tag{4.23}$$

Substituting $\sigma_r|_{r=\rho} = -p_\rho$ into equation (4.23) results in

$$\begin{aligned}-p_\rho &= -p\left(\frac{a}{\rho}\right)^{\frac{6\mu}{3+2\mu}} + 2\frac{\kappa\epsilon_{pa}^{m}}{3m-2\mu}\left(\left(\frac{a}{\rho}\right)^{\frac{6\mu}{3+2\mu}} - \left(\frac{a}{\rho}\right)^{\frac{9m}{3+2\mu}}\right)\\ &\quad -2c\frac{27(6-2\mu)\epsilon_{pa}}{(3+2\mu)^2(15-2\mu)}\frac{1}{a^2}\left(\left(\frac{a}{\rho}\right)^{\frac{6\mu}{3+2\mu}} - \left(\frac{a}{\rho}\right)^{\frac{15+4\mu}{3+2\mu}}\right)\end{aligned} \tag{4.24}$$

On the elasto-plastic interface the stress components given in equations (4.9) and (4.10) must satisfy the yield condition

$$\bar{\sigma}|_{r=\rho} = \sigma_y \tag{4.25}$$

Substituting the elastic stress solutions (4.9) and (4.10) and the yield condition (4.12) into equation (4.25) gives the internal pressure required to cause yielding at the internal boundary as

$$p_\rho = p_0 + \frac{2(\sigma_y + \mu p_0)(b^3 - \rho^3)}{3b^3 + 2\mu\rho^3} \tag{4.26}$$

Inserting equations (4.19) and (4.26) into equation (4.23) gives

$$\begin{aligned} p &= \left(p_0 + \frac{2(\sigma_y + \mu p_0)(b^3 - \rho^3)}{3b^3 + 2\mu\rho^3}\right)\left(\frac{a}{\rho}\right)^{\frac{6\mu}{3+2\mu}} \\ &+ 2\frac{\kappa}{3m - 2\mu}\left(\frac{\sigma_y}{E}\right)^m \left(\frac{\rho}{a}\right)^{\frac{9m}{3+2\mu}} \left(1 - \left(\frac{a}{\rho}\right)^{\frac{9m-6\mu}{3+2\mu}}\right) \\ &- 2c\frac{27(6-2\mu)}{(3+2\mu)^2(15-2\mu)}\frac{\sigma_y}{E}\left(\frac{\rho}{a}\right)^{\frac{9}{3+2\mu}} \frac{1}{a^2}\left(1 - \left(\frac{a}{\rho}\right)^{\frac{15-2\mu}{3+2\mu}}\right) \end{aligned} \tag{4.27}$$

Using equations (4.19), (4.23) and (4.27) gives the radial stress as

$$\begin{aligned} \sigma_r &= -\left(p_0 + \frac{2(\sigma_y + \mu p_0)(b^3 - \rho^3)}{3b^3 + 2\mu\rho^3}\right)\left(\frac{a}{\rho}\right)^{\frac{6\mu}{3+2\mu}} \\ &+ 2\frac{\kappa}{3m - 2\mu}\left(\frac{\sigma_y}{E}\right)^m \left(\left(\frac{\rho}{a}\right)^{\frac{6\mu}{3+2\mu}} - \left(\frac{\rho}{r}\right)^{\frac{9m}{3+2\mu}}\left(\frac{r}{a}\right)^{\frac{6\mu}{3+2\mu}}\right) \\ &- 2c\frac{27(6-2\mu)}{(3+2\mu)^2(15-2\mu)}\frac{\sigma_y}{E}\left(\frac{\rho}{a}\right)^{\frac{9}{3+2\mu}} \frac{1}{a^2}\left(\left(\frac{a}{\rho}\right)^{\frac{15-2\mu}{3+2\mu}} - \left(\frac{a}{r}\right)^{\frac{15-2\mu}{3+2\mu}}\right) \end{aligned} \tag{4.28}$$

The circumferential stress follows from equation (4.12) as

$$\sigma_\theta = \frac{3\bar{\sigma} + (3-\mu)\sigma_r}{3 + 2\mu} \tag{4.29}$$

Substituting equations (4.18) and (4.19) into equations (4.14) gives the strain components as

$$\epsilon_r = \left(-1 + \frac{\mu}{3}\right)\frac{\sigma_y}{E}\left(\frac{\rho}{r}\right)^{\frac{9}{3+2\mu}} \tag{4.30}$$

$$\epsilon_\theta = \left(\frac{1}{2} + \frac{\mu}{3}\right)\frac{\sigma_y}{E}\left(\frac{\rho}{r}\right)^{\frac{9}{3+2\mu}} \tag{4.31}$$

Finally, from the geometric equations (4.6) and equation (4.31) the radial displacement is obtained as

$$u = \left(\frac{1}{2} + \frac{\mu}{3}\right) \frac{r\sigma_y}{E} \left(\frac{\rho}{r}\right)^{\frac{9}{3+2\mu}} \tag{4.32}$$

All the necessary equations for the determination of the complete pressure expansion curve and the stress distributions have been derived. For given soil properties E, ν, μ, κ, m, σ_y, c, the internal pressure p and the radius ratio a_0/b_0. The continuity of the displacements at the elastic-plastic interface can be used to determine the radius of the elastic-plastic boundary ρ from equations (4.11) and (4.32). ϵ_{pa} and p_ρ can afterwards be obtained easily from equations (4.19) and (4.26). Using the above parameters, the elastic stress and strain distributions can therefore be obtained from equations (4.9)-(4.11).

Special case

For frictionless materials ($\phi = 0$), the Drucker-Prager criterion reduces to the von Mises criterion. The solutions for the stress, strain and displacements, based on the von Mises criterion, can be obtained by setting $\mu = 0$ in the respective expressions.

Equation (4.28) reduces to

$$\begin{aligned} \sigma_r &= -p_0 - \frac{2\sigma_y}{3}\left(1 - \frac{\rho^3}{b^3}\right) \\ &+ 2\left(\frac{\kappa}{3m}\left(\frac{\sigma_y}{E}\right)^m \left(1 - \frac{\rho^{3m}}{r^{3m}}\right) - \frac{6c}{5}\frac{\sigma_y}{E}\left(\frac{\rho}{a}\right)^3 \frac{1}{a^2}\left(\frac{a^5}{\rho^5} - \frac{a^5}{r^5}\right)\right) \end{aligned} \tag{4.33}$$

The strain and displacement components in (4.30)-(4.32) assume the following form

$$\epsilon_r = -\frac{\sigma_y}{E}\left(\frac{\rho}{r}\right)^3 \tag{4.34}$$

$$\epsilon_\theta = \epsilon_\varphi = \frac{1}{2}\frac{\sigma_y}{E}\left(\frac{\rho}{r}\right)^3 \tag{4.35}$$

$$u = \frac{1}{2}\frac{\sigma_y}{E}\frac{\rho^3}{r^2} \tag{4.36}$$

The solution by Gao (2003b) is recovered for the same problem with $p_0 = 0$.

4.3 Cavity expansion in cohesionless soils

As for the expansion of cavity in cohesive-frictional material, let a and b be the current internal and external radii, as shown in Figure 4.1, and let ρ be the radius of the plastic boundary. The soil consists of an elastic-perfectly plastic cohesionless Drucker-Prager material that obeys an associated flow rule. A strain gradient plasticity theory of the form proposed by Vardoulakis and Aifantis (1991) is used, which can be written as follows

$$f = \sqrt{J_2} + I_1\mu(\epsilon_p, \nabla^2\epsilon_p) \tag{4.37}$$

which is defined for the spherical cavity as

$$f = \sigma_\theta - \sigma_r + \frac{3\mu(\epsilon_p, \nabla^2\epsilon_p)}{3 + 2\mu(\epsilon_p, \nabla^2\epsilon_p)}\sigma_r \tag{4.38}$$

The friction coefficient μ is assumed to be a function of the effective plastic strain as

$$\mu = \mu_0 - c\nabla^2\epsilon_p \tag{4.39}$$

where μ_0 is the initial internal friction coefficient.

Elastic solution

The analysis of spherical cavity expansion in cohesionless soils is analogous to that for a spherical cavity in cohesive-frictional soils. The elastic solutions of this problem are given by the equations (4.4)-(4.11)

Plastic solution

After initial yielding takes place at the cavity wall, a plastic zone will form around the inner cavity wall with an increase in the applied pressure p. The outer radius of

the plastic zone is denoted by ρ. Within the plastic zone, the constitutive equations are given by

$$\begin{aligned} \epsilon_r &= \left(-1+\frac{1}{3}\mu_0\right)\epsilon_p \\ \epsilon_\theta &= \epsilon_\varphi = \left(\frac{1}{3}+\frac{1}{3}\mu_0\right)\epsilon_p \end{aligned} \tag{4.40}$$

Substituting equations (4.40) into equation (4.7) yields

$$\frac{d\epsilon_p}{\epsilon_p} = \frac{-9}{3+2\mu_0}\frac{dr}{r} \tag{4.41}$$

Integrating equation (4.41) from a to r and making use of (4.16) leads to

$$\epsilon_p = \epsilon_{pa}\left(\frac{a}{r}\right)^{\frac{9}{3+2\mu_0}} \tag{4.42}$$

Inserting equation (4.42) into equation (4.17) gives

$$\epsilon_{pa} = \frac{\sigma_y}{E}\left(\frac{\rho}{a}\right)^{\frac{9}{3+2\mu_0}} \tag{4.43}$$

Using the gradient-dependent form of (4.39) and introducing (4.43) leads to

$$\mu = \mu_0 - c\frac{9(6-2\mu_0)\epsilon_{pa}}{(3+2\mu_0)^2}\frac{1}{a^2}\left(\frac{a}{r}\right)^{\frac{15+4\mu_0}{3+2\mu_0}} \tag{4.44}$$

$$\frac{d\sigma_r}{\sigma_r} = \frac{-6\mu_0 r^{\frac{15+4\mu_0}{3+2\mu_0}} + 6\alpha}{(3+2\mu_0)r^{\frac{15+4\mu_0}{3+2\mu_0}} - 6\alpha}\frac{1}{r}dr \tag{4.45}$$

with α defined as

$$\alpha = c\frac{9(6-2\mu_0)\epsilon_{pa}}{(3+2\mu_0)^2}\frac{1}{a^2}a^{\frac{15+4\mu_0}{3+2\mu_0}} \tag{4.46}$$

After some algebraic manipulations, the differential equation is obtained as

$$\frac{d\sigma_r}{\sigma_r} = \frac{1}{3+2\mu_0}\left(\frac{-3(3+2\mu_0)}{r} + \frac{9r^{\frac{15+4\mu_0}{3+2\mu_0}-1}}{r^{\frac{15+4\mu_0}{3+2\mu_0}} - \frac{2\alpha}{3+2\mu_0}}\right)dr \tag{4.47}$$

A direct integration of the resulting differential equation (4.47) from a to r leads to

$$\sigma_r = -p\frac{a^3}{r^3}\left(\frac{r^{\frac{15+4\mu_0}{3+2\mu_0}} - \frac{2c}{3+2\mu_0}\frac{9(6-2\mu_0)\epsilon_{pa}}{(3+2\mu_0)^2}\frac{1}{a^2}a^{\frac{15+4\mu_0}{3+2\mu_0}}}{a^{\frac{15+4\mu_0}{3+2\mu_0}} - \frac{2c}{3+2\mu_0}\frac{9(6-2\mu_0)\epsilon_{pa}}{(3+2\mu_0)^2}\frac{1}{a^2}a^{\frac{15+4\mu_0}{3+2\mu_0}}}\right)^{\frac{9}{15+4\mu_0}} \tag{4.48}$$

Substituting $\sigma_r|_{r=\rho} = -p_\rho$ into equation (4.48) we obtain

$$-p_\rho = -p\frac{a^3}{\rho^3}\left(\frac{\rho^{\frac{15+4\mu_0}{3+2\mu_0}} - \frac{2c}{3+2\mu_0}\frac{9(6-2\mu_0)\epsilon_{pa}}{(3+2\mu_0)^2}\frac{1}{a^2}a^{\frac{15+4\mu_0}{3+2\mu_0}}}{a^{\frac{15+4\mu_0}{3+2\mu_0}} - \frac{2c}{3+2\mu_0}\frac{9(6-2\mu_0)\epsilon_{pa}}{(3+2\mu_0)^2}\frac{1}{a^2}a^{\frac{15+4\mu_0}{3+2\mu_0}}}\right)^{\frac{9}{15+4\mu_0}} \tag{4.49}$$

Initial yielding occurs first at the inner wall of the cavity when the stresses satisfy the yield condition (4.25) and this happens when the cavity pressure reaches the following value

$$p_\rho = \frac{(3+2\mu_0)b^3}{3b^3+2\mu_0\rho^3}p_0 \tag{4.50}$$

Inserting equations (4.50) into equation (4.49) gives

$$p = p_\rho\frac{\rho^3}{a^3}\left(\frac{a^{\frac{15+4\mu_0}{3+2\mu_0}} - \frac{2c}{3+2\mu_0}\frac{9(6-2\mu_0)\epsilon_{pa}}{(3+2\mu_0)^2}\frac{1}{a^2}a^{\frac{15+4\mu_0}{3+2\mu_0}}}{\rho^{\frac{15+4\mu_0}{3+2\mu_0}} - \frac{2c}{3+2\mu_0}\frac{9(6-2\mu_0)\epsilon_{pa}}{(3+2\mu_0)^2}\frac{1}{a^2}a^{\frac{15+4\mu_0}{3+2\mu_0}}}\right)^{\frac{9}{15+4\mu_0}} \tag{4.51}$$

Using equations (4.43), (4.48) and (4.51) gives the radial stress as

$$\sigma_r = -\frac{(3+2\mu_0)b^3p_0}{3b^3+2\mu_0\rho^3}\frac{\rho^3}{r^3}\left(\frac{r^{\frac{15+4\mu_0}{3+2\mu_0}} - \frac{2c}{3+2\mu_0}\frac{9(6-2\mu_0)}{(3+2\mu_0)^2}\frac{1}{a^2}\frac{\sigma_y}{E}\left(\frac{\rho}{a}\right)^{\frac{9}{3+2\mu_0}}a^{\frac{15+4\mu_0}{3+2\mu_0}}}{\rho^{\frac{15+4\mu_0}{3+2\mu_0}} - \frac{2c}{3+2\mu_0}\frac{9(6-2\mu_0)}{(3+2\mu_0)^2}\frac{1}{a^2}\frac{\sigma_y}{E}\left(\frac{\rho}{a}\right)^{\frac{9}{3+2\mu_0}}a^{\frac{15+4\mu_0}{3+2\mu_0}}}\right)^{\frac{9}{15+4\mu_0}} \tag{4.52}$$

The circumferential stress follows from equations (4.38) and (4.52) as

$$\sigma_\theta = -\frac{(3-\mu_0)b^3p_0}{3b^3+2\mu_0\rho^3}\frac{\rho^3}{r^3}\left(\frac{r^{\frac{15+4\mu_0}{3+2\mu_0}} - \frac{2c}{3+2\mu_0}\frac{9(6-2\mu_0)}{(3+2\mu_0)^2}\frac{1}{a^2}\frac{\sigma_y}{E}\left(\frac{\rho}{a}\right)^{\frac{9}{3+2\mu_0}}a^{\frac{15+4\mu_0}{3+2\mu_0}}}{\rho^{\frac{15+4\mu_0}{3+2\mu_0}} - \frac{2c}{3+2\mu_0}\frac{9(6-2\mu_0)}{(3+2\mu_0)^2}\frac{1}{a^2}\frac{\sigma_y}{E}\left(\frac{\rho}{a}\right)^{\frac{9}{3+2\mu_0}}a^{\frac{15+4\mu_0}{3+2\mu_0}}}\right)^{\frac{9}{15+4\mu_0}} \tag{4.53}$$

Finally, the strain components and the radial displacement are obtained as

$$\epsilon_r = \left(-1+\frac{\mu_0}{3}\right)\frac{\sigma_y}{E}\left(\frac{\rho}{r}\right)^{\frac{9}{3+2\mu_0}} \tag{4.54}$$

$$\epsilon_\theta = \left(\frac{1}{2}+\frac{\mu_0}{3}\right)\frac{\sigma_y}{E}\left(\frac{\rho}{r}\right)^{\frac{9}{3+2\mu_0}} \tag{4.55}$$

$$u = \left(\frac{1}{2}+\frac{\mu_0}{3}\right)\frac{r\sigma_y}{E}\left(\frac{\rho}{r}\right)^{\frac{9}{3+2\mu_0}} \tag{4.56}$$

All the necessary equations for the determination of the complete pressure-expansion curve and the stress distributions have been derived for given values of the soil properties E, ν, μ, σ_y, c, the internal pressure p and the radius ratio a_0/b_0. This is accomplished by using the continuity of the displacements at the elastic-plastic boundary to determine the radius of the elastic-plastic boundary ρ from equations (4.11) and (4.56). ϵ_{pa} and p_ρ can afterwards be obtained easily from equations (4.43) and (4.50). Using the above parameters, the elastic stress and strain distributions can be obtained from equations (4.9)-(4.11).

4.4 Applications

In order to verify the problem solutions and implementations and to illustrate the features of the gradient plasticity models, a number of simulations are performed. In this analysis, the soil is assumed to be dry or fully drained and, the radius of the region analyzed is set to 500 times the initial radius a of the expanding cavity so that an infinite soil body can be modeled. For the initial conditions, the pressure p_0 = 50 kPa is taken in all the cases.

Consider the internal length scale l and assume that l is a function of the gradient related coefficient c and the shear modulus G as (Al Hattamleh et al., 2004)

$$l = \sqrt{\frac{c}{G}} \tag{4.57}$$

To perform the above calculations, a simple computer code written in FORTRAN is used. For varying cavity pressure p, the code calculates the stresses, strains and displacement as functions of the cavity radius using an iterative procedure.

An illustrative flow chart for the load stepping of the elasto-plastic cavity expansion is shown in Figure 4.2.

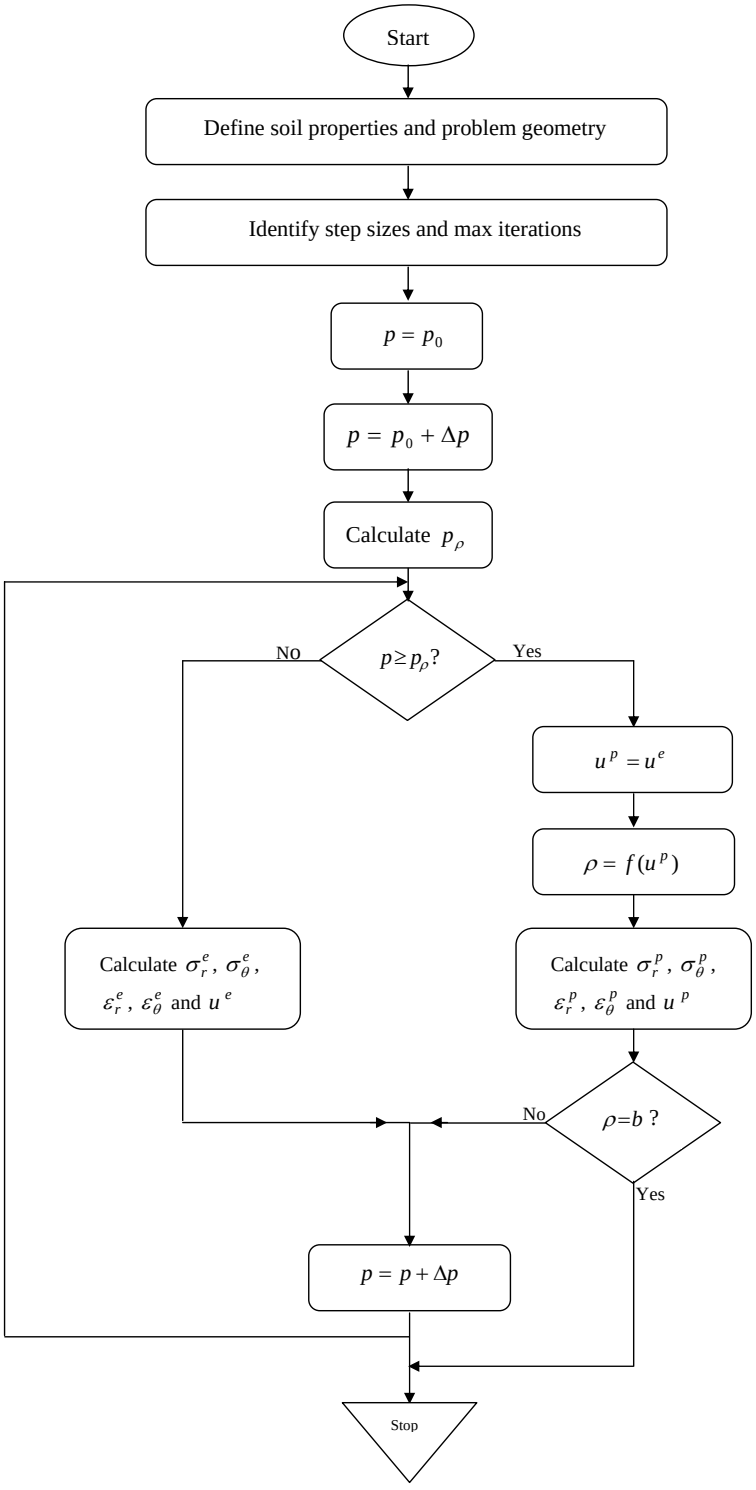

Figure 4.3: Flow chart for the load stepping of elastoplastic cavity expansion

Cohesive-Frictional soils

In the analysis of an expanding cavity in cohesive-frictional material, a constant value of the friction angle is adopted, only the cohesion exhibits the gradient-dependence. The parameter m that appears in the expression of the flow stress is assumed to be 0. The yield function in (4.1) is expressed therefore as

$$f = \sqrt{J_2} + \mu I_1 - (\beta c_0 - c\nabla^2 \epsilon_p) \tag{4.58}$$

were μ and β are functions of the internal friction angle ϕ (Yu, 2006)

$$\mu = \frac{2\sin\phi}{\sqrt{3}(3-\sin\phi)} \tag{4.59}$$

$$\beta = \frac{6\cos\phi}{\sqrt{3}(3-\sin\phi)} \tag{4.60}$$

and c_0 is the initial cohesion. The value of μ and β are defined in a way to match the Drucker-Prager yield surface with the Mohr-Coulomb yield surface at the triaxial compression (Figure 3.5).

A simulation is carried out with the material properties listed in Table (4.1). The pressure-expansion curves are presented in terms of normalized pressure p/p_0 and normalized cavity radius a/a_0. Noting that the main particle size d_{50} is used as the internal length scale l.

The size effect can be appreciated by considering various values of the parameter l/a. Noting that the case $l/a = 0$ in Figure 4.4 corresponds to classical plasticity theory ($c = 0$) and implies a very large cavity radius compared to the internal length. Figure 4.4 displays the evolution of the normalized pressure with the increase of the normalized cavity radius. It is clear that the material exhibits higher resistance as the cavity radius decreases. In fact, for a given material with constant l, the smaller is the size the stronger is the response.

Table 4.1: Cohesive-frictional soil parameters

Young's modulus	E = 18.5 MPa
Poisson ratio	$\nu = 0.2$
Friction angle	$\phi = 25\ ^\circ$
initial cohesion	$c_0 = 15.5$ kPa
Yield stress	$\sigma_y = 500$ kPa
Length scale	$d_{50} = 0.02$ mm

Figure 4.5 shows the influence of the material length on the pressure-expansion curve. With the increasing value of the material length parameter, the strength of the material increases significantly. If the strain gradient effect is neglected, all curves will reduce to a single curve.

The normalized limit pressure vs. the cavity radius a is depicted in Figure 4.6. The curves are evaluated for both classical ($c = 0$) and gradient theories. It is clearly seen that the limit pressure is size dependent when the inner radius a is small. For large diameter (on the order of 1 mm or above), the limit pressure approaches a limit value, which can be obtained from the classical theory of cavity expansion. Obviously, this scale dependence cannot be predicted by the classical theory, since the constitutive equation does not contain any term with length scale.

Cohesionless soils

To investigate the size dependence of the cohesionless material response, numerical calculations are carried out using the parameters listed in Table (4.2). In Figure 4.7 remarkable difference in the pressure-expansion curves can be observed. The limit pressures exhibit a distinctive size effect with the increase of the initial cavity radii. As for the expansion of cavity in cohesive-frictional material, the value $l/a =$

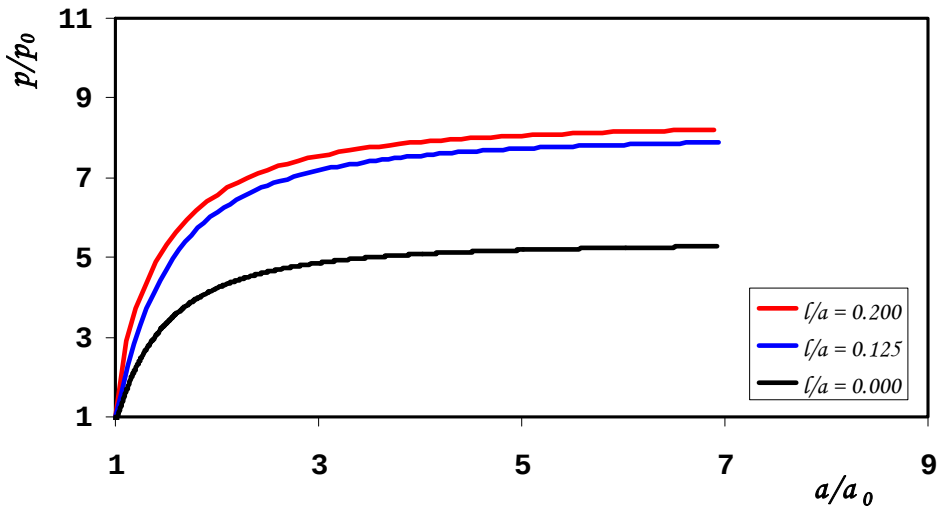

Figure 4.4: Variation of the pressure-expansion response with the cavity radius for cohesive-frictional soil, l=0.02 mm

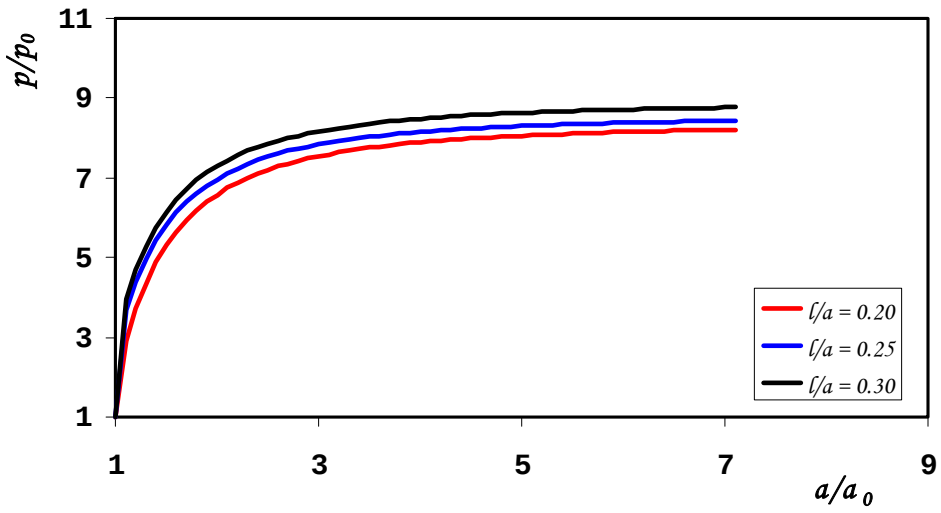

Figure 4.5: Variation of the pressure-expansion response with the material length scale for cohesive-frictional soil, a_0=0.1 mm

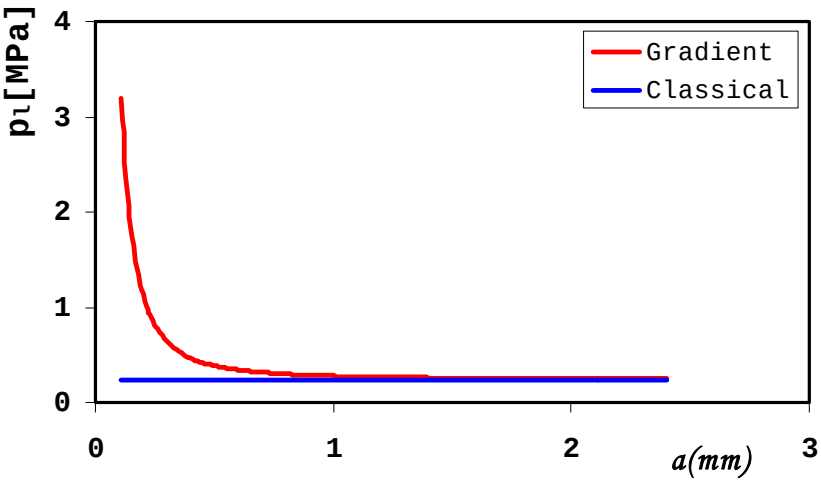

Figure 4.6: Variation of the normalized limit pressure with the cavity radius for cohesive-frictional soil

Table 4.2: Cohesionless soil parameters

Young's modulus	E = 80 MPa
Poisson ratio	$\nu = 0.3$
Friction angle	$\phi = 35\ ^\circ$
Yield stress	$\sigma_y = 500$ kPa
Length scale	$d_{50} = 1.5$ mm

0 corresponds to the classical plasticity theory ($c = 0$), which indicates a very large cavity radius comparable to the material length scale.

Figure 4.8 contains a representative plot of the normalized pressure as a function of the normalized cavity radius for increasing material length l. The numerical results illustrate that when the length parameter takes different values, the material response curves are different and the material strength increases with the increase of the length parameter.

Shown in Figure 4.9 are theoretical predictions of the normalized limit pressures

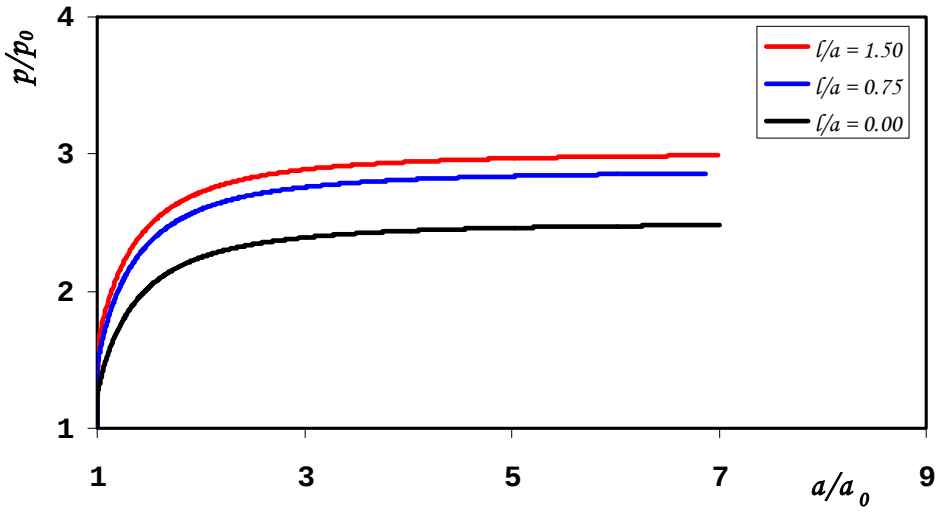

Figure 4.7: Variation of the pressure-expansion response with the cavity initial radius for the cohesionless soil, l=1.5 mm

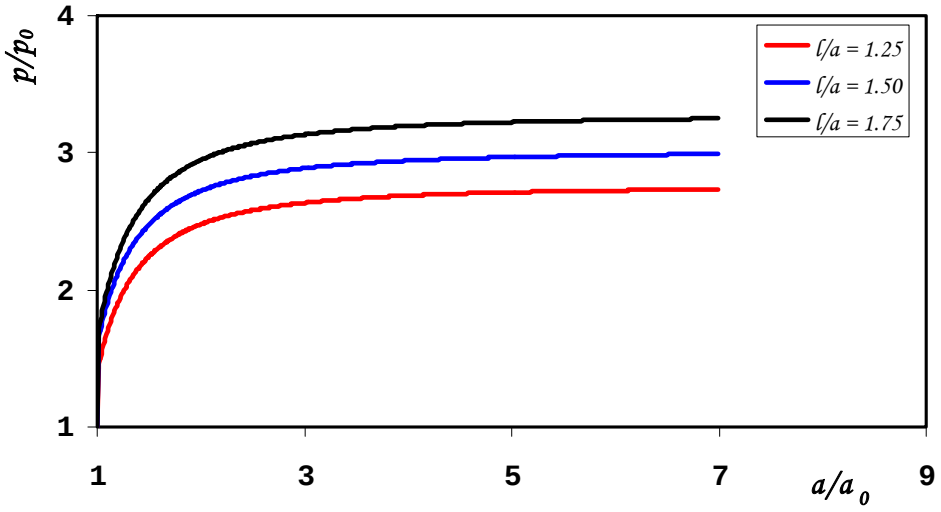

Figure 4.8: Variation of the pressure-expansion response with the length scale for the cohesionless soil, a_0=1 mm

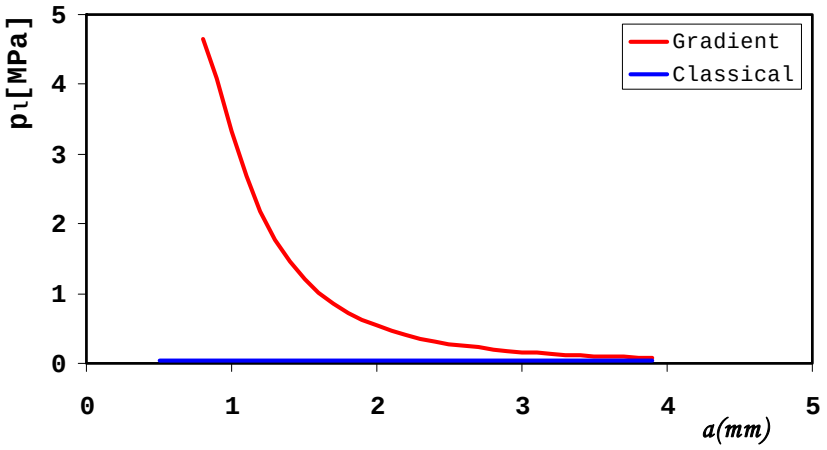

Figure 4.9: Variation of the normalized limit pressure with the cavity radius for the cohesionless soil.

for both classical and gradient materials. The gradient materials show an increase in the limit pressure with decreasing cavity radius, while no size effect is observed for the classical ones. This size effect is not captured by classical theory, according to which the material response should remain constant.

4.5 Conclusion

The framework of strain gradient plasticity theory is used to solve the cavity expansion problem for cohesive-frictional and for cohesionless materials obeying the associated Drucker-Prager yield criterion. Analytical solutions are presented to study the size effects through the incorporation of a length scale in the constitutive description.

We demonstrate that the penetration pressure required to expend a cavity in soil depends on the ratio between the cavity size and the mean grain diameter of the soil particles. This implies that the enhanced gradient theory is successful in capturing the size effects for small cavities, where the internal length introduced by the gradient coefficient is comparable to the cavity size. Obviously, this size dependence cannot

be predicted by the classical theory, since the constitutive equation does not contain any term with length scale.

The results in this chapter show that the solution of cavity expansion with gradient plasticity theory captures the salient features of scale effect fairly well in a qualitative manner, since the material parameters are assumed without being calibrated with experiments. In the next chapter, some experimental results are presented and compared with the theoretical prediction.

Chapter 5

Experimental investigation and analysis

5.1 Introduction

A number of soil testing methods have been developed to determine soil properties in field, static cone penetration test (CPT) is one of the most popular techniques used for this purpose. CPT was first used by the Swedish State Railways in about 1917 in a study on the bearing resistance of pile foundation in sand (Meigh, 1987). Since then, cone penetrometers are widely used especially when further improvements have been incorporated, e.g. the standarized design and size of the apparatus, measurement procedure and data interpretation (Hignett, 2002). While in geotechnical engineering mainly large penetrometers are used, small sized penetrometers have been developed for material characterization in agriculture engineering. Miniature cone penetrometres are used to deduce soil properties and their resistance to root growth. These penetrometeres often have a diameter ranging from a few millimeters to about two centimeters.

Numerous correlations linking soil parameters to the measured penetration re-

sistance have been proposed and they are based on empirical or analytical methods, in which the cavity expansion methods are commonly used. The relation between cavity expansion theory and cone penetration test is based on the assumption that the movement of a blunt probe ($\alpha \succ 30\ ^\circ$) through the soil creates a spherical cavity around the cone tip. For sharp penetrometers ($\alpha \prec 5\ ^\circ$), a cylindrical cavity enlargement model is more appropriate (Greacen and Sands, 1980; Whiteley and Dexter, 1981).

In conventional plasticity theory, in which material is treated as a continuum, the cavity stress and displacement fields are independent of the absolute geometry size. Experiments show, however, that the penetrometer pressure depends on the penetrometer diameter in the way that, the smaller is the probe diameter the stronger is the soil response (Whiteley and Dexter, 1981). However, the test data in the literature are rare. Therefore, we decide to carry out own tests to substantiate our theory.

This chapter presents the results of a series of penetration tests using penetrometer probes with diameters of 2, 5 and 10 mm (see Figure 5.1). The tests were performed on loose and dense sand samples under dry conditions. The aim of this chapter is to investigate the effects of the strain gradient in the penetration of the probes and, to check whether the gradient plasticity model can capture the size dependence in penetration tests.

5.2 Soil samples

In order to establish the effect of the penetrometer size on the soil response, some penetration tests are performed on coarse silica dry sand. The mean grain size (d_{50}) is approximately 0.9 mm, which is determined by dry sieving. The sand is filled into a cylindrical mould (8.3 cm in diameter and 14 cm in length) under both loose and

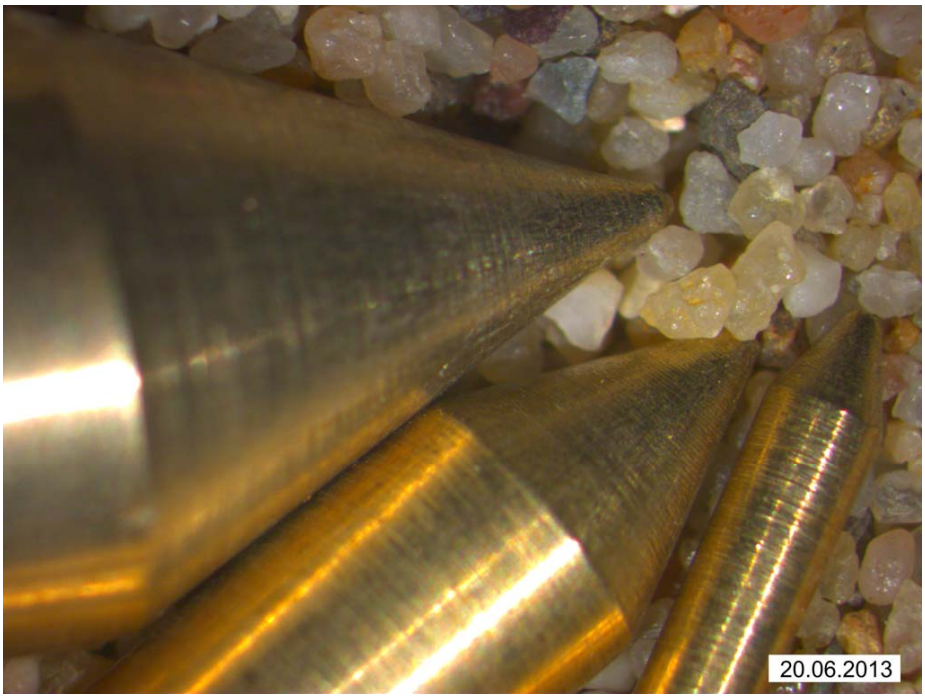

Figure 5.1: Penetrometers used in the experiments

dense conditions. Sand densities of 1.60 kg/cm^3 and 1.75 kg/cm^3 were obtained by measuring the volume of the cylinder and the dry weight of the sand.

5.3 Test Apparatus

The experiments were conducted using a computer-controlled electro mechanical testing machine (Zwick/Roell, Zmart.Pro), using a 50 N load cell. This machine is normally used for tensile and/or compression tests on different materials like metals and synthetic materials. It was adjusted to the specific needs for our experiment. Its construction consists of a vertical frame that guides a horizontal placed movable traverse (Figure 5.2). For the penetration test, the penetrometer is attached at right angles to the end of the load cell. (Figure 5.3).

Figure 5.2: Testing machine (Zwick/Roell, Zmart.Pro)

Figure 5.3: Penetrometer attached to the load cell

5.4 Test procedure and data processing

The tests were performed in the laboratory of Physics and Materials Science at the University of Natural Resources and Life Sciences, Vienna. In all experiments the penetration force of three steel probes of diameters d of 2, 5 and 10 mm and 60 ° point angle is measured (Figure 5.3). The tests consist of pushing the penetrometers into the sand samples at a constant speed of 3 mm/min from $z = 0$ down to about 7-8 d. The frictional force is estimated by measuring the force required to retract the probe from the soil after the penetration test is completed. The force acting on the cone is calculated by subtracting the frictional force from the total force. Each test (probe diameter and sand density) is repeated ten times under the same conditions to obtain a main load along the depth. The tests show excellent reproduceability.

The data acquisition and the control of the testing machine was performed using the software TestXpert II. The displacement was measured with a displacement transducer.

5.5 Analysis of penetration data

The cone tip resistance q_c is defined as the vertical force acting on the cone divided by the projected area of the cone ($q_c = F/A$). Calculation is based on the main value of q_c of ten tests. In order to estimate the ultimate resistance, the cone penetration resistance is averaged over selected intervals of depth (Poplin, 1965). The depth interval is chosen to be approximately one probe diameter. In Figures 5.4 to 5.9 the statistical results of the cone penetration tests are presented.

For the purpose of statistical analysis, the main cone penetration results over selected intervals of depth are found to be approximately constant at depths greater than 5 times d for all penetrometer probes. The ultimate cone resistance is obtained

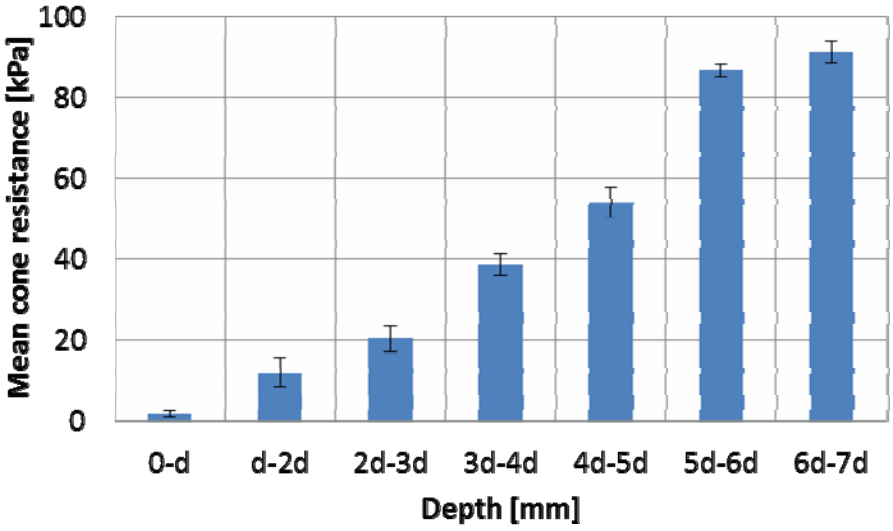

Figure 5.4: Mean penetration resistance for 2 mm diameter probe in loose sand (10 penetration replicates). Error bars show ± standard error of results.

by averaging cone resistances data at depths greater than this.

In order to check the presented gradient plasticity model for cohesionless materials (Section. 4.3), numerical simulations of cone penetration tests have been carried out and compared to the experimental results.

By expanding a cavity of finite radius, a limiting pressure σ is achieved. This limiting pressure is related to the cone tip stress q_c as follows

$$q_c = \sigma(1 + \tan\phi \cot\alpha) \tag{5.1}$$

where $\alpha = 30°$ is the cone semi-angle and $\tan\phi$ is the coefficient of soil-probe friction. This parameter ($\tan\phi$) is taken as 0.20 for loose sand and as 0.22 for dense sand (Tejchman, 1989).

The material parameters entering the scale dependent constitutive equation are estimated approximately from the triaxial tests conducted by Schöfer (2012) with loose and dense sand. These parameters are listed in the Table 5.1. Noting that the yield stress σ_y is obtained from the intersection of the tangent line of the initial

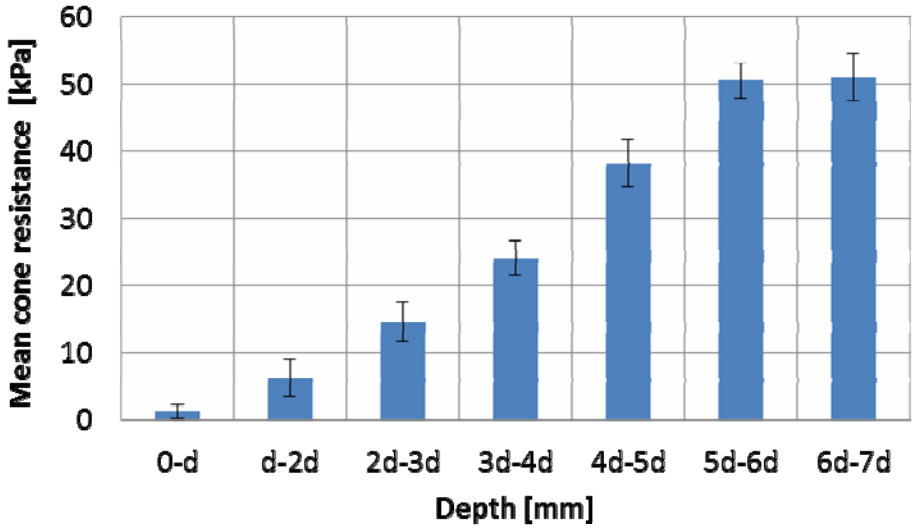

Figure 5.5: Mean penetration resistance for 5 mm diameter probe in loose sand (10 penetration replicates). Error bars show ± standard error of results.

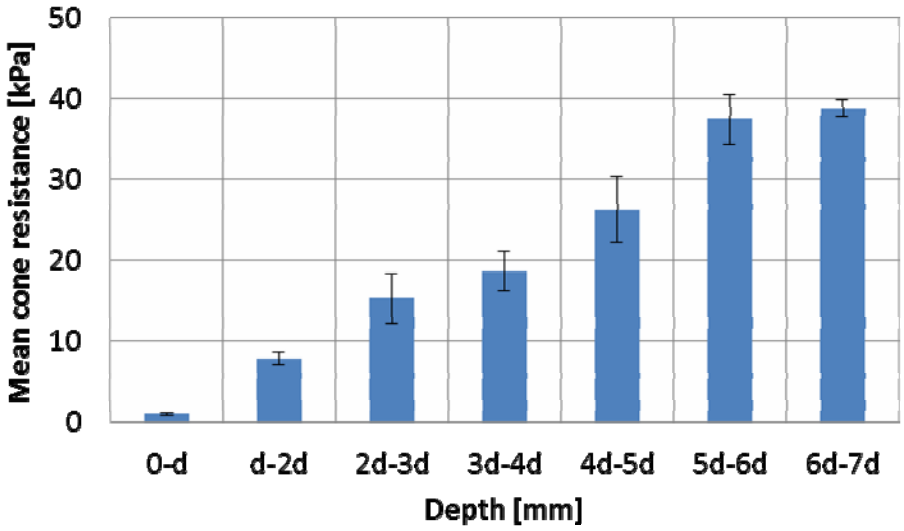

Figure 5.6: Mean penetration resistance for 10 mm diameter probe in loose sand (10 penetration replicates). Error bars show ± standard error of results.

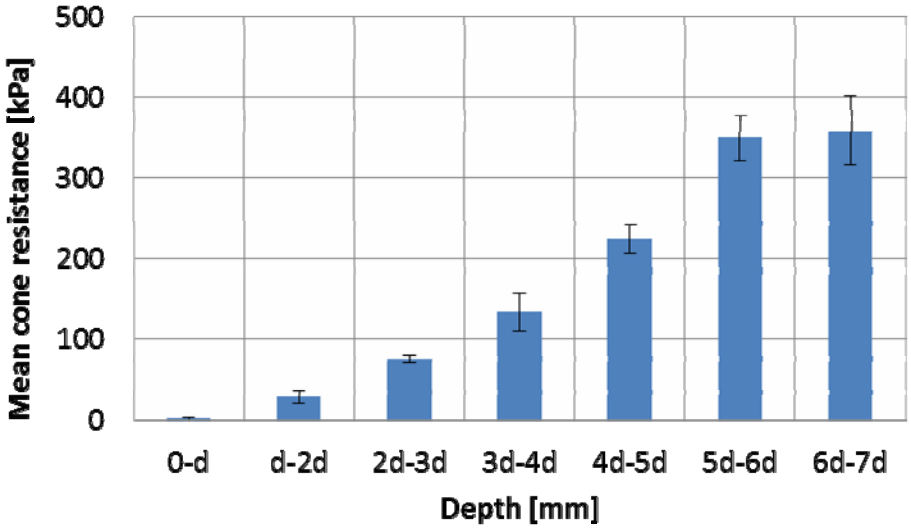

Figure 5.7: Mean penetration resistance for 2 mm diameter probe in dense sand (10 penetration replicates). Error bars show ± standard error of results.

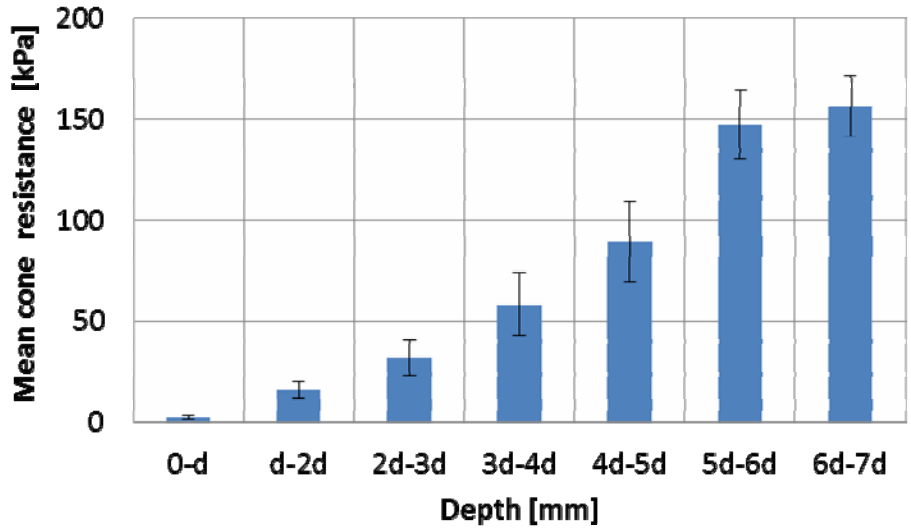

Figure 5.8: Mean penetration resistance for 5 mm diameter probe in dense sand (10 penetration replicates). Error bars show ± standard error of results.

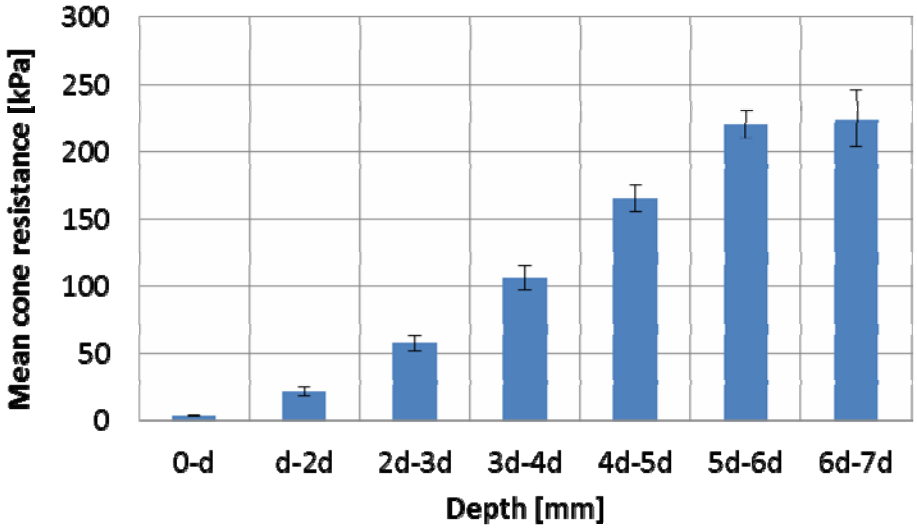

Figure 5.9: Mean penetration resistance for 10 mm diameter probe in dense sand (10 penetration replicates). Error bars show ± standard error of results.

portion with the line tangent to the stress-strain curve at large displacement for loose sand. For dense sand, the yield stress is obtained from the intersection of the initial tangent line with the horizontal line of the maximum stress.

Table 5.1: Soil parameters for numerical calculations

	E [MPa]	ν	ϕ [°]	σ_y [kPa]	d_{50} [mm]
Loose sand	10	0.3	33	330	0.9
Dense sand	30	0.4	38	520	0.9

The initial stress p_0 is assumed to be equal to the horizontal stress $\sigma_H = K_0 \gamma z$ acting at depth z, where K_0 is the coefficient of earth pressure at rest [$\approx (1 - \sin\phi)$] and γ is the unit weight of the sand. This is the stress that acts on the plane perpendicular to the penetration direction (Houlsby and Hitchman, 1988).

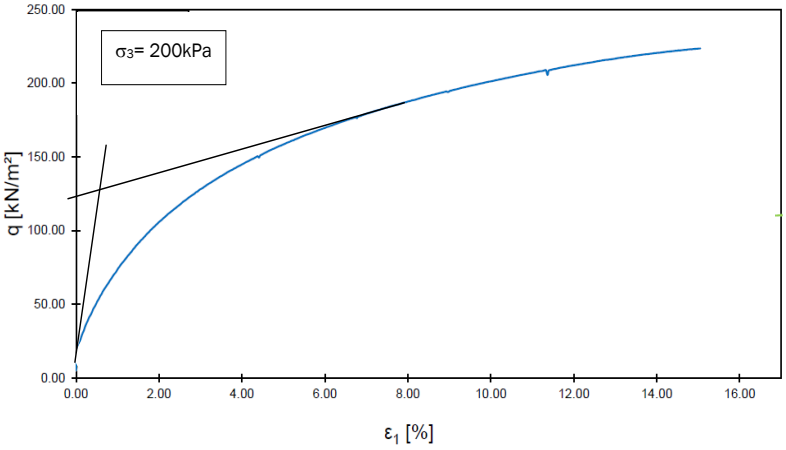

Figure 5.10: Yield stress for loose sand

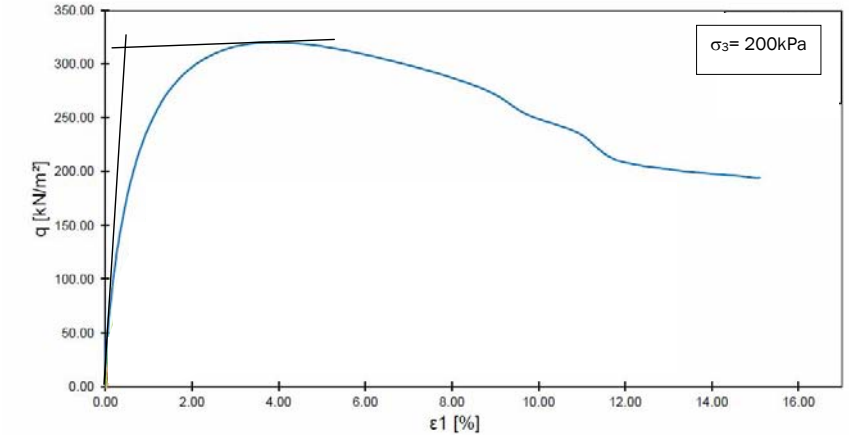

Figure 5.11: Yield stress for dense sand

5.6 Results and discussion

In Figures 5.12 and 5.13 the cone penetrometer resistance calculated using the strain gradient theory are plotted against penetrometer area together with the experimental results. According to the results, it can be seen that the cone resistance are affected by the penetrometer sizes. The penetration resistance for the probe of 2 mm diameter is about 45% greater than that of the 5 mm probe for loose sand and of about 56% greater for dense sand. It is also shown that as the penetrometer diameter increases, the two curves representing the experimental results as well as that representing the predicted results converge approximately to a value, which seems to be independent of the penetrometer size.

As a second remark on the test results, the effect of the bulk density of the sand samples on the cone resistance using the different penetrometers is clearly seen in the curve represented in Figure 5.14 . An increase of the bulk density leads to increased cone pressure for the two sand samples. For example, for 2 mm probe diameter, the difference between the cone penetration resistance for dense and loose is about 73%. This indicates that for dense sand, the forces necessary to move or rearrange the particles of the soil by the penetrometer tends to be higher.

Statistical analysis (Coefficient of determination R^2, Absolute error) was used for comparison between the theoretical predictions and experimental results for soil penetration resistance. A simple linear regression analysis was conducted using Microsoft Excel 2010 to determine whether there is a correlation between the results (Figures 5.15 and 5.16). The best fit to the experimental data was found with the loose sand with a coefficient of determination R^2 of 0.98 and an absolute error of 0.01 (see Figure 5.15). A perusal of Figure 5.16 shows that the difference between theory and experiment is larger for dense sand. This may be due to the fact that the measured cone resistance with 10 mm diameter is found to be greater than that

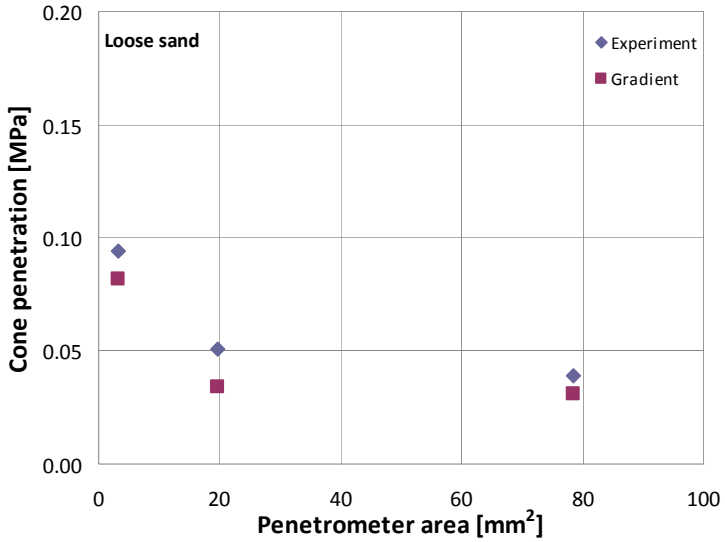

Figure 5.12: Cone penetration resistance vs. penetrometer area for loose sand

measured with 5 mm probe which is not predicted theoretically. The difference between the predicted and measured values of the cone resistance may be because the effect of the chamber size and boundary conditions. Schnaid and Houlsby (1991) studied the effect of the chamber ratio (the diameter of the chamber divided by the diameter of the cone) and found out that the effect of the chamber ratio is more pronounced for dense and medium sand. A significant effect was also reported in centrifuge tests on dense sand for a chamber ratio of about 8.85 (Bolton et al., 1999). The results may also have been caused by the influence of cone to particle size ratio. Gui and Bolton (1998) studied this effect in centrifuge tests on dense coarse sand and concluded that a grain size effect was found when ratio falls below about 20.

5.7 Conclusion

A set of three probes with diameters of 2, 5 and 10 mm was used to perform CPT on loose and on dense dry sand samples. After statistical evaluations, the ultimate cone tip resistance is determined from the profile of CPT data by taking the main cone

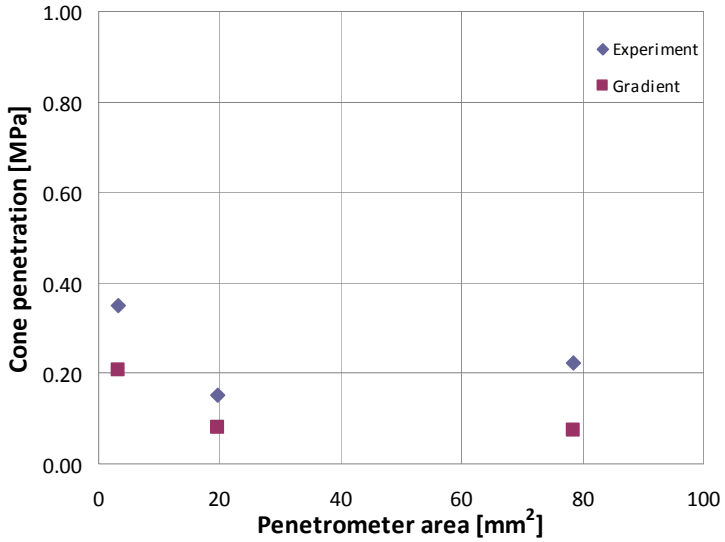

Figure 5.13: Cone penetration resistance vs. penetrometer area for dense sand

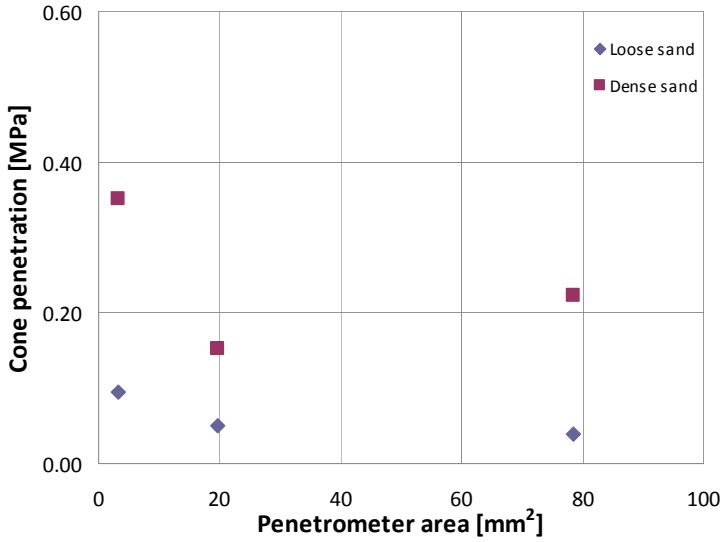

Figure 5.14: Dependence of cone penetration on the bulk density

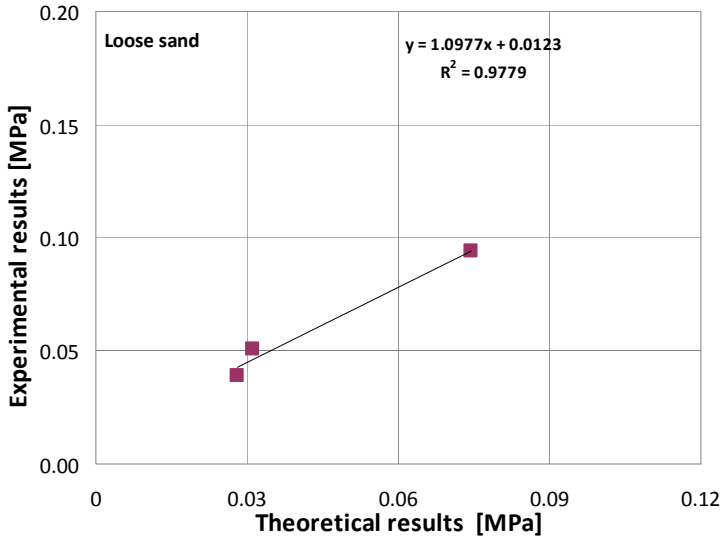

Figure 5.15: Comparison between theoretical and experimental results for loose sand

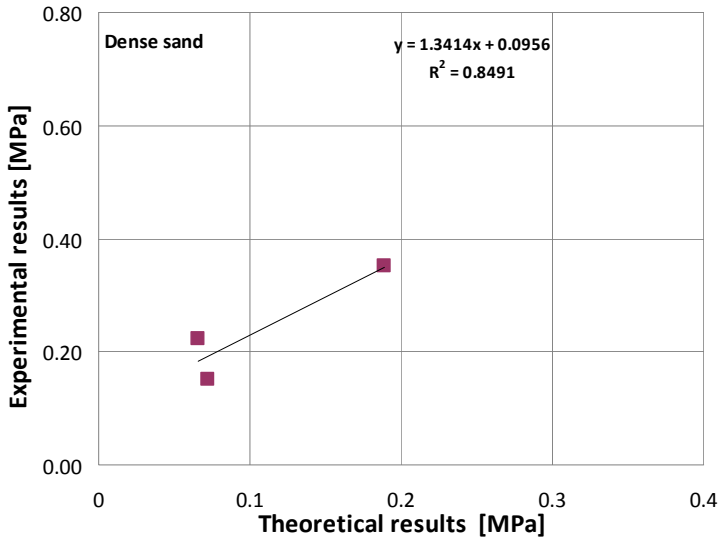

Figure 5.16: Comparison between theoretical and experimental results for dense sand

tip resistance at a depth greater than 5 times of probe diameter. A strain gradient plasticity theory is used to simulate the penetration precess in order to study the feature of the theory to predict the size effects in penetration tests. Comparison between the theoretical predictions and experimental results shows good agreement. The tests on loose sand show better agreement with the theory than dense sand. Better agreement between the predicted and measured responses could be achieved if the boundary conditions and grain size effects were taken into account.

The increase of the penetrometer diameter is associated by a decrease of the penetration resistance. For large diameter, the pressure is expected to approach a limit value, which is independent of the penetrometer size. Moreover, the tests show that the penetrometer resistance increases with increasing sand bulk density. Larger force is required to penetrate through compacted soil. This indicates that the penetration resistance varies not only with the size of the probe but also with the density of the soil.

Chapter 6

General discussion and conclusions

This dissertation presented a formulation of two gradient plasticity models to simulate the penetration of plant roots into compacted soils. Considering that root growth is analogous to the expansion of spherical cavity, an elastoplastic analysis for cavity expansion in cohesive-frictional and in cohesionless soils is investigated. The soil is modeled as an elastic-perfectly plastic material, its elastic response is assumed to obey the Hooke's law and its yielding is determined by the associated Drucker-Prager yield criterion. The analysis of the numerical results leads to the conclusion that the penetration pressure required to expand a cavity in soil depends on the ratio between the cavity size and the mean grain diameter of the soil particles. Within the framework of the classical theory of cavity expansion, the penetration force is proportional to the cross section of the root and therefore, an increase in root diameter does not provides any advantage. Due to the introduction of a material length into the constitutive relationship, it is shown that the cavity pressure exhibits a distinctive size effect with the increase of the cavity size in the way that, the smaller is the cavity size the stronger is the soil response. In addition, an increase of the expansion response is shown for increasing the material length parameter. The models show also a largely stronger gradient dependent response

that is not accounted for by the classical theory. In both models, the solutions approach the classical solutions asymptotically if the internal length introduced by the gradient coefficient is small comparable to the cavity size.

The effect of the characteristic material length as well as the effect of the cavity size were previously studied within the framework of the strain gradient theory. Existing solutions of the cavity expansion problem vary because of differences in the constitutive models for the stress-strain behavior of the expanding body (Gao, 2003a; Gao, 2003b; Tsagrakis et al., 2006; Zhao, Sheng and Sloan, 2007; Zhao, 2011). However, no applications of this theory are known to cavity size effects using Drucker-Prager yield criterion. Gao (2003a, b) has developed an analytical solutions of the cavity expansion problems using strain gradient plasticity theory with power-law hardening and von-Mises yield criterion. These solutions have been successfully used to analyze the size effects in terms of the maximum effective stress. Since the Drucker-Prager yield criterion is an extension of the von-Mises yield criterion to account for the hydrostatic stress, the solution presented in this thesis for cohesive-frictional soils reduces to the solutions of Gao (2003b) for the same problem. It is noted that, Gao (2003b) did not employ his solution to investigate the influences of the cavity size and the microstructural properties on the pressure-expansion response, which are presented in our study. Similar cavity size dependence behavior was also captured by Tsagrakis et al. (2006) for internally pressurized thick-walled hollow cylinder using both deformation and flow theories. The stress-strain curves show a decreasing material response with increasing cavity size for the both theory versions.

Using the strain gradient theory of the form proposed by Fleck and Hutchinson (1997, 2001) in conjunction with the Mohr-Coulomb yield criterion, Zhao (2011) has developed a numerical method to solve both cylindrical and spherical cavity expan-

sion problems in micromorphic media. His work is a generalization of a previous work presented by Zhao, Sheng and Sloan (2007). In order to investigate the effect of the internal length scale on the expansion response, Zhao (2011) found that the use of larger values of internal length scale produces a stronger pressure-expansion curve. However, in contrast to our study, he found that the ultimate pressures at the fully plastic yielding stage appear to be roughly the same for all cases of the internal length scales, but he did not give any explanation to the observed response.

Other theories are also used to solve the cavity expansion problem such as strain gradient elasticity (Collin, Caillerie and Chambon, 2009; Gao, Park and Ma, 2009) and strain gradient elastoplasticity (Zervos, Papanastasiou and Vardoulakis, 2001). These theories introduce also gradient terms of the strain in the evolution equations for state variables. Collin, Caillerie and Chambon (2009) proposed an analytical solution for the thick-walled cylinder problem of an isotropic elastic second gradient medium. They showed that in micro-scales the stresses in a homogenous cylinder are completely different from the values predicted by classical elasticity when the microstructure effects become predominant (i.e. the internal length scale is much larger than the thickness of the cylinder). Gao, Park and Ma (2009) have derived a closed-form solution using a simplified strain gradient elasticity theory. The authors have concluded that microstructural effects can be quantitatively large and the classical elasticity solution may not be accurate for materials exhibiting significant microstructure dependence. Zervos, Papanastasiou and Vardoulakis (2001) have introduced an elastic and a plastic material length parameters in the elastoplastic governing equations. In order to predict the existence of the cavity size effect, the authors have shown that the scale effect fades out rapidly with increasing cavity size. In concluding remarks, it is noted that the results of many of the previous solutions are in agreement with the results presented in this study, which proves

the applicability of our solutions. Finally, it should be also noted that many of the previous works did not experimentally test the solutions proposed.

In order to validate the model formulation presented in our work for cohesionless soils , a selection of results obtained from laboratory experiments on penetrometer with 2, 5 and 10 mm diameters is compared with the simulations of the expanding cavity. Statistical manipulations were derived to estimate the ultimate cone tip resistance from the profile of CPT data. A Goodness of fit analysis including the coefficients of determination and the absolute errors were performed to compare the predicted and measured results. It is shown that the model predicts cone tip pressure values that are in remarkable agreement with the experimental results. The best fit to the experimental data was found with the loose sand with a coefficient of determination R^2 of 0.98. Better correlation between the predicted and measured responses could be achieved for dense sand if the boundary conditions and grain size effects were taken into account. This implies the capability of the gradient approach to capture the size dependence of the soil response better than with the conventional theory. This latter is shown to be a special case when the dimension of the microstructure is negligible compared with the cavity size.

This study provides a further explanation for root thickening. Larger root diameter gives rise to lower penetration pressure. The driving force is known to be provided by the turgor pressure in the root cells. When faced with increasing mechanical impedance, plant roots may choose either to increase the turgor pressure while keeping the root diameter unchanged or to increase the root diameter while keeping the turgor pressure unchanged. Plant root may of course increase both the diameter and the turgor pressure simultaneously. Note that the turgor pressure (about 1 MPa) is not unlimited and is mainly dictated by the behavior of the cell walls. Therefore, it makes sense to increase the root diameter instead of the turgor

pressure. Some experiments in plant science indicate that the turgor pressure does not show remarkable change when roots are mechanically impeded (Clark, Whalley and Barraclough, 2003). For constant turgor pressure, the penetration force will be proportional to the cross section area of the roots. However, root growth is enhanced by the reduced penetration resistance from the soil. Finally, it should be noticed that the interaction between root and soil is not purely mechanical. In general, compaction changes not only the mechanical strength of soil but also its water potential, which requires hydro-mechanically coupled analyses.

Some additional qualitative aspects could be investigated for further research. The first consists to account for the non-associative mechanical behavior of the soil, which is needed to capture properly the inelastic volume effects (dilatancy). As it will be difficult to solve this problem analytically, the proposed constitutive models and the modified form of governing equations can be implemented into a finite element code.

Additionally, the initial material properties used in the models are assumed to be constant throughout the simulation. To this end, a constitutive law that properly accounts for the changes of these parameters is required. Moreover, the influence of soil microstructure on the elastic properties of the soil can be further investigated.

Experimental works can be carried out done for other types of soils, taking into consideration the grain size and the chamber size effects as well as the water content of the soil at different confining pressure, thereby the usefulness of the two models developed in this thesis can be validated. More work should be also done for the determination of the model parameters and the gradient term from the tests results.

Bibliography

[1] Abdalla, A.M., Hettiaratchi, D.R.P., Reece, A.R.: The mechanics of root growth in granular media. *J. agric. Engng. Res.*, 14:236-248, 1969.

[2] Aggarwal, G.C., Prihar, S.S.: A simple technique to determine axial root growth force. *Plant and Soil*, 42:485-489, 1975.

[3] Aifantis, E.C.: On the microstructural origin of certain inelastic models. *J. Eng. Mat. Tech.*, ASME, 106:326-330, 1984.

[4] Aifantis, E.C.: The Physics of Plastic Deformation, *Int. J. Plasticity*, 3:211-247, 1987.

[5] Aifantis, E.C.: Strain gradient interpretation of size effects. *Int. J. Fracture*, 95:299-314, 1999.

[6] Aifantis, E.C.: Update on a class of gradient theories. *Mechanics of Materials*, 35:259-280, 2003.

[7] Al Hattamleh, O., Muhunthan, B., Zbib, H.M.: Gradient plasticity modelling of strain localization in granular materials. *Int. J. Numer. Anal. Meth. Geomech.*, 28:465-481, 2004.

[8] Alehossein, H., Korinets, A.: Mesh-independent finite difference analysis using gradient-dependent plasticity. *Comm. Num. Meth. Eng.*, 16:363-375, 2000.

[9] Atwell, B.J.: Physiological responses of lupin roots to soil compaction. *Plant and Soil* 111, 277-281 (1988)

[10] Atwell, B.J.: The effect of soil compaction on wheat during early tillering. I. Growth, development and root structure. *New Phytol.*, 115:29-35, 1990.

[11] Barley, K.P.: Effects of root growth and decay on the permeability of a synthetic sandy loam. *Soil Science*, 78:205-210, 1954.

[12] Barley, K.P.: Influence of soil strength on growth of roots. *Soil Science*, 96:175-180, 1963.

[13] Barley, K. P., Farrell, D., Greacen, E. L.: The influence of soil strength on the penetration of a loam by plant roots. *Aust. J. Soil Res.*, 3:69-79, 1965.

[14] Barley, K. P., Greacen E. L.: Mechanical resistance as a soil factor influencing the growth of roots and underground shoots. *Adv. Agron.*, 19:1-43, 1967.

[15] Bažant, Z.P., Pijaudier-Cabot, G.: Nonlocal continuum damage, localization instability and convergence. *J. Applied Mechanics*, Transactions ASME 55:287-293, 1988.

[16] Becher, H.H.: Soil compaction around a small penetrating cylindrical body and its consequences. *Soil Technology*, 7:83-91, 1994.

[17] Beilby, M.J., Bisson, M.A., Shepherd, V.A.: The electrophysiology of turgor regulation in charophyte cells. In: Volkov AG editor. Plant electrophysiology-theory and methods. Elsevier, New York, 2006.

[18] Bengough, A.G., Mullins, C.E.: Mechanical impedance to root growth: a review of experimental techniques and root growth responses. *J. Soil Science*, 41:341-358, 1990a.

[19] Bengough, A.G., Mullins, C.E.: The resistance experienced by roots growing in a pressurized cell. A reappraisal. *Plant and Soil*, 123:73-82, 1990b.

[20] Bengough, A.G., Mullins, C.E.: Penetrometer resistance, root penetration resistance and root elongation rate in two sandy loam soils. *Plant and Soil*, 131:59-66, 1991.

[21] Bengough, A.G., Mullins, C.E., Wilson, G.: Estimating soil frictional resistance to metal probes and its relevance to the penetration of soil by roots. *European J. of Soil Science*, 48:603-612, 1997.

[22] Bengough, A.G., Campbell, D.J., OSullivan, M.F.: Penetrometer techniques in relation to soil compaction and root growth. In: Smith KA, Mullinsed CE (eds) Soil and environmental analysis: physical methods, 2nd edn. Marcel Dekker, New York, NY, 377-403, 2001.

[23] Bengough, A.G.: Root growth and function in relation to soil structure, composition and strength. In: de Kroon H., Visser E.J.W. (eds.): Root Ecology Springer-Verlag, Berlin: 151-171, 2003.

[24] Bengough, A.G., Croser, C., Pritchard J.: A biophysical analysis of root growth under mechanical stress. *Plant and Soil*, 189:155-164, 1997.

[25] Bengough, A.G., Mackenzie, C.J., Elangwe, H.E.: Biophysics of the growth responses of pea roots to changes in penetration resistance. *Plant and Soil*, 167:135-141, 1994.

[26] Bishop, R. F., Hill, R., Mott, N. F.: Theory of indentation and hardness tests. *Proc. Phys. Sot.*, 57:147-159, 1945.

[27] Bolton, M.D., Gui, M.W., Garnier, J., Corte, J.F., Bagge, G., Laue, J., Renzi, R.: Centrifuge cone penetration tests in sand. *Géotechnique*, 49:543-552, 1999.

[28] Bradford, J.M., Farrell, D.A., Larson, W.E.: Effect of soil overburden pressure on penetration of fine metal probes. *Soil Sci. Soc. Am. Proc.*, 35:12-15, 1971.

[29] Carter, J.P., Booker, J.R., Yeung, S.K., Cavity expansion in cohesive frictional soils. *Géotechnique*, 36:349-358, 1986.

[30] Chadwick, P.: The quasi-static expansion of a spherical cavity in metals and ideal soils. *Q. J. Mech. Appl. Math.*, 12:52-71, 1959.

[31] Chen,J.S, Wu, C.T., Belytschko, T.:Regularization of material instabilities by meshfree approximations with intrinsic length scales. *Int. J. Num. Meth. Eng.*, 47:1303-1322, 2000.

[32] Clark L.J., Whalley, W.R., Barraclough P.B.: How do roots penetrate strong soil?. *Plant and Soil*, 255:93-104, 2003.

[33] Clark, L.J., Bengouhg, A.G., Whalley, W.R., Dexter, A.R., Barrclough, P.B.: Maximum axial root growth pressure in pea seedlings: effects of measurement techniques and cultivars. *Plant and soil*, 209:101-109, 1999.

[34] Clark, L.J., Barraclough, P.B.: Do dicotyledons generate greater maximum axial root growth pressures than monocotyledons? *J. Exp. Bot.*, 50:1263-1266, 1999.

[35] Cockroft, B., Barley, K.P., Greacen, E.L.: The penetration of clays by fine probes and root tips. *Aust. J. Soil Res.*, 7:333-48, 1969.

[36] Coleman, B.D., Hodgdon, M.L.: On shear bands in ductile materials. Archive of Rational Mechanics and Analysis. 90:219-247, 1985.

[37] Collis-George, N., Williams, J.: Comparison of the effects of soil matric potential and isotropic effective stress on the germination of Lactura Sativa. *Aust. J. Soil Res.*, 6:179-192, 1968.

[38] Collin, F., Caillerie, D., Chambon, R.: Analytical solutions for the thick-walled cylinder problem modeled with an isotropic elastic second gradient constitutive equation. *Int. J. Solids Struct.*, 46:3927-3937, 2009.

[39] Collins, I.F., Yu, H.S.: Undrained cavity expansions in critical state soils. *Int. J. Numer. Anal. Meth. Geomech.*, 20:489-516, 1996.

[40] Croser, C., Bengough, A.G., Pritchard, J.: The effect of mechanical impedance on root growth in pea (Pisum sativum). I. Rates of cell flux, mitosis, and strain during recovery. *Physiologia Plantarum*, 107:277-286, 1999.

[41] Croser, C., Bengough, A.G., Pritchard, J.: The effect of mechanical impedance on root growth in pea (Pisum sativum). II. Cell expansion and wall rheology during recovery. *Physiologia Plantarum*, 109:150-159, 2000.

[42] Cudmani. R., Osinov, V.A.: The cavity expansion problem for the interpretation of cone penetration and pressuremeter tests. *Can. Geotech. J.*, 38:622-638, 2001.

[43] de Borst, R., Mühlhaus, H.: Gradient-dependent plasticity: formulation and algorithmic aspects. *Int. J. Num. Meth. Eng.*, 35:521-539, 1992.

[44] de Borst, R., Pamin, J.: Some novel developments in finite element procedures for gradient-dependent plasticity. *Int. J. Num. Meth. Eng.*, 39:2477-2505, 1996.

[45] de Borst, R., Sluys, L.J.: Localisation in a Cosserat continuum under static and dynamic loading conditions. *Comput. Meth. Appl. Mech. Eng.*, 90:805-827, 1991.

[46] Desrues, J., Chambon, R., Mokni, M., Mazerolle, F.: Void ratio evolution inside shear bands in triaxial sand specimens studied by computed tomography. *Géotechnique*, 46:529-546, 1996.

[47] Desrues J., Lanier J., Stutz P.: Localization Of the deformation in tests on sand sample . *Eng. fracture mechanics*, 21:909-921, 1985.

[48] Dexter, A.R.: Compression of soil around roots. *Plant and Soil*, 97:401-406, 1987.

[49] Dickison, W.C.: Integrative plant anatomy. Integrative plant anatomy. Elsevier USA (2000).

[50] Donald, R.G., Kay, B.D., Miller, M.H.: The effect of soil aggregate size on early shoot and root growth of maize (Zea mays L.). *Plant and Soil*, 103:251-259, 1987.

[51] Durban, D., Fleck, N.A.: Spherical cavity expansion in a drucker-prager solid. *J. Appl. Mech.*, 64:743-750, 1997.

[52] Engelen, R.A.B., Geers, M.G.D., Baajens, F.P.T.: Nonlocal implicit gradient-enhanced elasto-plasticity for the modelling of softening behaviour. *Int. J. Plasticity*, 19:403-433, 2003.

[53] Evans, G.N.: A technique of simulation of radial root growth in soil and some experimental results. *Soil Science*, 109:376-387, 1970.

[54] Farrell, D.A., Greacen, E.L.: Resistance to penetration of fine probes in compressible soil. *Aust. J. Soil Res.*, 4:1-17, 1966.

[55] Fitter, A.H.: Characteristics and functions of root systems, in: Waisel Y., Eshel A., Kafkafi U. Eds., Plant Roots. The Hidden Half, 3rd ed., Marcel Dekker, Inc., New York, 2150, 1996.

[56] Fleck, N. A., Muller, G.M., Ashby, M.F., Hutchinson, J. W.: Strain gradient plasticity: Theory and experiment. *Acta Metallurgica et Materialia*, 42:475-487, 1994.

[57] Fleck, N. A., Hutchinson, J. W.: Strain gradient plasticity. *Adv. Appl. Mech.*, 33:295-361, 1997.

[58] Fleck, N. A., Hutchinson, J. W.: A reformulation of strain gradient plasticity. *J. Mech. Phys. Solids*, 49:2245-2271, 2001.

[59] Forbes, J.C., Watson, R.D.: Plants in Agriculture. Cambridge University Press, Cambridge, 1992.

[60] Gao, X.L.: Elasto-plastic analysis of an internally pressurized thick-walled cylinder using a strain gradient plasticity theory. *Int. J. Solids and Structures*, 40:6445-6455, 2003a.

[61] Gao, X.L.: Strain gradient plasticity solution for an internally pressurized thick walled spherical shell of an elastic-plastic material. *Mech. Res. Comm.*, 30:411-420, 2003b.

[62] Gao, X.L., Park, S., Ma, H.: Analytical solution for a pressurized thick-walled spherical shell based on a simplified strain gradient elasticity theory. *Math. Mech. Solids*, 14:747-758, 2009.

[63] Gibson, R.E., Anderson, W.F.: In-situ measurement of soil properties with the pressuremeter. *Civil Eng. Public Works Rev.*, 56:615-618, 1961.

[64] Goodman, A.M., Ennos, A.R.: The effect of soil bulk density on the morphology and anchorage mechanics of the root systems of sunflower and maize. *Annals of Botany*, 83:293-302, 1999.

[65] Goss, M.J., Russel, R.S.: Effects of mechanical impedance on root growth in barley (Hordeum vulgare L.). III: Observations on the mechanism of response. *J. Exp. Bot.*, 31:577-588, 1980.

[66] Greacen, E.L., Farrell, D.A., Forrest, J.A.: Measurement of density patterns in Soil. *J. agric. Engng. Res.*, 12:311-313, 1967.

[67] Greacen, E.L., Sands, R.: Compaction of Forest Soils. A review. *Aust. J. Soil Res.*, 18:163-89, 1980.

[68] Greacen, E.L., Oh, J.S.: Physics of root growth. *Nature New Biology*, 235:24-25, 1972.

[69] Gregory, P.J.: Plant Roots: Growth, Activity and Interaction with Soils. Blackwell Publishing, Oxford, 2006.

[70] Gui M.W., Bolton M.D.: Geometry and scale effects in CPT and pile design. *Proceedings 1st International Conference on Site Characterisation, ISC '98, Atlanta*, 1063-1068, 1998.

[71] Harris, H.G., Sabnis, G.M.: Structural Modeling and Experimental Techniques, Second Edition, CRC Press, 1999.

[72] Hawes, M.C., Bengough, A.G., Cassab, G., Ponce, G.: Root caps and rhizosphere. *J. Plant Growth Regul.*, 21:352-367, 2003.

[73] Hill, R.: The mathematical theory of plasticity, Oxford University Press, London, England, 1950.

[74] Houlsby, G.T., Hitchman, H.: Calibration chamber tests of a cone penetrometer in sand. *Géotechnique*, 38:39-44, 1988.

[75] Houlsby, G.T., Withers, N.J.: Analysis of the cone pressuremeter test in clay. *Géotechnique*, 39:575-587, 1988.

[76] Iijima, M., Kato, J.: Combined soil physical stress of soil drying, anaerobiosis and mechanical impedance to seedling root growth of four crop species. *Plant Prod. Sci*, 10:451-459, 2007.

[77] Iijima, M., Higuchi, T., Barlow, P.W., Bengough, A.D.: Root cap removal increases root penetration resistance in maize (Zea mays L.). *J. Exp. Bot.*, 54:2105-2109, 2003.

[78] Kirby, J.M., Bengough, A.G.: Influence of soil strength on root growth: experiments and analysis using critical-state model. *European J. of Soil Science*, 53:119-128, 2002.

[79] Klepper, B.: Development and growth of crop root systems. In: Hatfield JL, Stewart BA, Eds., Limitations to plant root growth. Springer-Verlag, Berlin, 1992.

[80] Leyser,O., Day, S.: Mechanisms in plant development. Blackwell Science Ltd., 2003.

[81] Logsdon, S.D., Parker, J.C., Reneau, R.B.: Root growth as influenced by aggregate size. *Plant and Soil*, 99:267-275, 1987.

[82] Materechera, S.A., Dexter, A.R., Alston.: Penetration of very strong soils by seedling roots of different plant species. *Plant and Soil*, 135:31-41, 1991.

[83] Materechera, S.A., Alston, A.M., Kirby, J.M., Dexter, A.R.: Influence of root diameter on the penetration of seminal roots into a compacted subsoil. *Plant and Soil*, 144:297-303, 1992.

[84] Materechera, S.A., Alston, A.M., Kirby, J.M., Dexter, A.R.: Field evaluation of laboratory techniques for predicting the ability of roots to penetrate strong soil and of the influence of roots on water sorptivity. *Plant and Soil*, 149:149-158, 1993.

[85] Meyerhof, G.G.: The ultimate bearing capacity of foundations. *Géotechnique*, 2:301-332, 1951.

[86] Misra, R.K., Dexter, A.R., Alston, A.M.: Maximum axial and radial growth pressures of plant roots. *Plant and Soil*, 95:315-326, 1986a.

[87] Misra, R.K., Dexter, A.R., Alston, A.M.: Penetration of soil aggregates of finite size - I. Blunt penetrometer probes. *Plant and Soil*, 94:43-58, 1986b.

[88] Misra, R.K., Dexter, A.R., Alston, A.M.: Penetration of soil aggregates of finite size - II. Plant roots. *Plant and Soil*, 94:59-85, 1986c.

[89] Misra, R.K., Alston, A.M., Dexter, A.R.: Root growth and phosphorus uptake in relation to the size and strength of soil aggregates. I: Experimental studies. *Soil Tillage Res.*, 11:103-116, 1988.

[90] Mitchell, A.R., Ellsworth, T.R., Meek, B.D.: Effect of root systems on preferential flow in swelling soil. *Comm. Soil Sci. Plant Anal.*, 26:2655-2666, 1995.

[91] Mühlhaus, H., Aifantis, E.C.: A variational principal for gradient plasticity. *Int. J. Solids Struct.*, 28:845-857, 1991.

[92] Mühlhaus, H.-B., Vardoulakis, I.: Thickness of shear bands in granular materials. *Géotechnique*, 37:271-283, 1987.

[93] Nabors, M. W.: Introduction to botany. Pearson/Benjamin Cummings, San Francisco, 2004.

[94] Nakai, T.: Constitutive Modelling of Geomaterials: Principles and Applications. CRC Press, 2013.

[95] Nix, W.D.: Mechanical properties of thin films. *Metallurgical Transactions A*, 20A:1989-2217, 1989.

[96] Osinov, V.A., Cudmani, R.: Theoretical investigation of the cavity expansion problem based on a hypoplasticity model. *Int. J. Numer. Anal. Meth. Geomech.*, 25:473-495, 2001.

[97] Palmer, A.C.: Undrained plane-strain expansion of a cylindrical cavity in clay: a simple interpretation of the pressuremeter test, *Géotechnique*, 22:451-457, 1972.

[98] Pamin, J., de Borst, R.: A gradient plasticity approach to finite element predictions of soil instability. *Arch. Mech.*, 47:353-377, 1995.

[99] Pamin J.: Gradient-dependent plasticity in numerical simulation of localization phenomena. Ph.D. dissertation, Delft University of Technology, Delft,1994,

[100] Passioura, J.B: Soil conditions and plant growth. *Plant, Cell and Environment*, 25:311-318, 2002.

[101] Peerlings R.H.J., de Borst R., Brekelmans W.A.M., Geers M.G.D.: Gradient enhanced modeling of concrete fracture. *Mech. Cohes. Frict. Mater.*, 3:323-342, 1998,

[102] Pfeffer, W.: Druck und Arbeitsleistung durch wachsende Pflanzen. *Abhandlungen der Königlich. Sächsischen Gesellschaft der Wissenschaften*, 33:235-474, 1893.

[103] Pierret, A., Moran, C.J., Pankhurst, C.E.: Differentiation of soil properties related to the spatial association of wheat roots and soil macroportes. *Plant and Soil*, 211:51-58, 1999.

[104] Poplin, J.K.: Statistical Evaluation of cone penetration test data. Miscellaneous paper, U.S. Army Engineer Waterways Experiment Station. 1965.

[105] Pritchard, J.: The control of cell expansion in roots. *New Phytol.*, 127:3-26, 1994.

[106] Randolph, M.F., Carter, J.P., Wrath, C.P.: Driven piles in clay -the effects of installation and subsequent consolidation. *Géotechnique*, 29:361-393, 1979.

[107] Raven, J.A., Edwards, D.: Roots: evolutionary origins and biogeochemical significance. *J. Exp. Bot.*, 52:381-401, 2001.

[108] Rice, J.R.: The localization of plastic deformation. Proc. 14th Int. Congress on Theoretical and Applied Mech., Delft, the Netherlands, W. T. Koiter, ed., 1, 207-220, 1976.

[109] Richards, B.G., Greacen, E.L.: Mechanical stresses on an expanding cylindrical root analogue in granular media. *Aus. J. Soil Res.*, 24:393-404, 1986.

[110] Richards, C.W.: Effect of size on the yielding of mild steel beams. *Proceedings of the American Society for Testing and Materials*, 58:955-970, 1958.

[111] Roscoe, K.H.: The influence of strains in soil mechanics. *Géotechnique*, 20:129-170, 1970,

[112] Rudnicki, J.W., Rice, J.R.: Conditions for the localization of deformation in pressure sensitive dilatant materials. *J. Mech. Phys. Solids*, 23:371-394, 1975.

[113] Schnaid, F., Houlsby, G.T.: An assessment of chamber size effects in the calibration of in situ tests in sand. *Géotechnique*, 41:437-445, 1991.

[114] Scholefield, D., Hall, D.M.: Constricted growth of grass roots through rigid pores. *Plant and Soil*, 85:153-162, 1985.

[115] Schöfer, D.: Untersuchung der Scherparameter eines Feinmittelsandes im gesättigten und teilgesättigten Zustand. Diplomarbeit an der Universität für Bodenkultur, Wien, 2012.

[116] Schreyer, H.L., Chen, Z.: One-dimensional softening with localization. *J. Appl. Mech.* ASME 53:791-797, 1986.

[117] Shuttle, D.A., Jefferies, M.G.: Dimensionless and unbiased CPT interpretation in sand. *Int. J. Numer. Anal. Meth. Geomech.*, 22:351-391, 1998.

[118] Salgado, R., Mitchell, J.K., Jamiolkowski, M.: Cavity Expansion and Penetration Resistance in Sand. *J. Geotech. Geoenviron. Eng.*, ASCE, 123:344-354, 1997.

[119] Souty, N.: Aspect mécanique de la croissance des racines. I. - Mesure de la force de pénétration. *Agronomie*, 7:623-630, 1987

[120] Stirzaker, R.J., Passioura, J.B., Wilms, Y.: Soil structure and plant growth. Impact of buklk density and biopores. *Plant and Soil*, 185:151-162, 1996.

[121] Stölken, J., Evans, A.: A microbend test method for measuring the plasticity length scale. *Acta Materialia*, 46:5109-5115, 1998.

[122] Stolzy, L.H., Barley, K.P.: Mechanical resistance encountered by roots entering compact soils. *Soil Science*, 105:297-301, 1968.

[123] Tatsuoka, F., Nakamura, S., Huang, C.C., Tani, K.: Strength anisotropy and shear band direction in plane strain tests of sand. *Soils and Found.*, 30:35-54, 1990.

[124] Taylor, H.M., Burnett, E.: Influence of Soil Strength on the Root-Growth Habits of Plants. *Soil Science*, 98:174-180, 1963.

[125] Taylor, H.M., Roberson, G.M., Parker, J.J: Soil strength-root penetration relations for medium- to coarse-textured soil materials. *Soil Science*, 102:18-22, 1966.

[126] Tejchman J., Wu, W.: Numerical simulation of shear band patterning in bi-axial compression tests. *Mechanics Research Communications*, 20:15-24, 1993.

[127] Tejchman J.: Scherzonenbildung und Verspannungseffekte in Granulaten unter Berücksichtigung von Korndrehungen. Veröffentlichungen des Institutes für Bodenmechanik und Felsmechanik der Universität Fridericiana in Karlsruhe, 117. 1989.

[128] Tsagrakis, I., Efremidis, G., Konstantinidis, A., Aifantis, E.C.: Deformation vs. flow and wavelet-based models of gradient plasticity: examples of axial symmetry. *Int. J. Plasticity*, 22:1456-1485, 2006.

[129] Tsegaye, T., Mullins, C.E.: Effect of mechanical impedance and morphology of two varieties of growth pea (Pisum sativum L.). *New Phytol.*, 126:707-713, 1994.

[130] Vardoulakis, I., Aifantis, E.C.: Gradient dependent dilatancy and its implication in shear banding. *Ingenieur Archiv*, 59:197-208, 1989.

[131] Vardoulakis, I., Aifantis, E.C.: A gradient flow theory of plasticity for granular materials. *Acta Mechanica*, 87:197-217, 1991.

[132] Vardoulakis, I., Graf, B.: Calibration of constitutive models for granular materials using data from biaxial experiments. *Géotechnique*, 35:299-317, 1985.

[133] Vardoulakis, I., Sulem, J.: Bifurcation Analysis in Geomechanics, Chapman and Hall, 1995.

[134] Veen, B.W.: The influence of mechanical impedance on the growth of maize roots. *Plant and Soil*, 66:101-109, 1982.

[135] Vesic, A.S.: Expansion of Cavities in Infinite Soil Mass. *J. Soil Mech. Fdn. Div., Proc.*, ASCE, 98:265-290, 1972.

[136] Vesic, A.S.: Design of Pile Foundations, Synthesis of Highway Practice 42, Transportation Research Board, National Research Council, Washington, D.C., 1977.

[137] Whally, W.R., Dumitru, E., Dexter, A.R.: Biological effects of soil compaction. *Soil Tillage Res.*, 35:53-68, 1995.

[138] Whiteley, G.M., Dexter, A.R.: The dependence of soil penetrometer pressure on penetrometer size. *J. agric. Engng. Res.*, 26:467-476, 1981.

[139] Whiteley, G.M., Dexter, A.R.: Behavior of roots in cracks between soil peds. *Plant and Soil*, 74:153-162, 1983a.

[140] Whiteley, G.M., Dexter, A.R.: Displacement of soil aggregates by elongating roots and emerging shoots of crop plants. *Plant and Soil*, 77:131-140, 1983b.

[141] Whiteley, G.M., Dexter, A.R.: Displacement of soil aggregates by elongating roots and emerging shoots of crop plants. *Plant and Soil*, 77:131-140, 1984.

[142] Wiersum, L.K.: The relationship of the size and structural rigidity of pores to their penetration by roots. *Plant and Soil*, 9:75-85, 1957.

[143] Young, I.M.: Biophysical interactions at the root-soil interface: a review. *J. agric. Engng. Res.*, 130:1-7, 1998.

[144] Yu, H.S.: Cavity Expansion Theory and its Application to the Analysis of Pressuremeters, Ph.D. Thesis, Oxford University, 1990.

[145] Yu, H.S.: Cavity Expansion Methods in Geomechanics, Kluwer Academic Publishers, 2000.

[146] Yu, H.S.: Plasticity and Geotechnics, Springer, New York, 2006.

[147] Yu, H.S., Houlsby, G.T.; Finite cavity expansion in dilatant soils: loading analysis. *Géotechnique*, 41:173-183, 1991.

[148] Zbib, H.M., Aifantis, E.C.: On the localization and post-localization behavior of plastic deformation. I. On the initiation of shear bands. *Res. Mechanica*, 23:261-305, 1988.

[149] Zbib, H.M., Aifantis, E C.: On the gradient-dependent theory of plasticity and shear banding, *Acta Mechanica*, 92:209-225, 1992.

[150] Zhao, J.D.: A Unified theory for cavity expansion in cohesive-frictional micromorphic media. *Int. J. Solids Struct.*, 48:1370-1381, 2011.

[151] Zhao, J.D., Sheng, D.C., Sloan, S.W: Cavity expansion of a gradient-dependent soil cylinder. *Int. J. Solids Struct.*, 44:4342-4368, 2007.

[152] Zhu, H.T., Zbib, H.M., Aifantis, E.C.: Strain gradients and continuum modeling of size effect in metal matrix composites. *Acta Mech.*, 121:165-176, 1997.